

# A Thermoelastic Transversely Isotropic Thick Walled Cylinder/Disk Application: An Analytical Solution and Study

S.M. Arnold  
*Lewis Research Center*  
*Cleveland, Ohio*

October 1989

(NASA-TM-102320) A THERMOELASTIC  
TRANSVERSELY ISOTROPIC THICK WALLED  
CYLINDER/DISK APPLICATION: AN ANALYTICAL  
SOLUTION AND STUDY (NASA) 46 p CSCL 20K

N90-12950

Unclas  
G3/39 0240384

**NASA**



# A THERMOELASTIC TRANSVERSELY ISOTROPIC THICK WALLED CYLINDER/ DISK APPLICATION: AN ANALYTICAL SOLUTION AND STUDY

S.M. Arnold  
National Aeronautics and Space Administration  
Lewis Research Center  
Cleveland, Ohio 44135

## ABSTRACT

A continuum theory is utilized to represent the thermoelastic behavior of a thick walled composite cylinder that can be idealized as transversely isotropic. A multi-axial statement of the constitutive theory employed is presented, as well as, the out of the plane of isotropy, plane stress and plane strain reductions. The derived analytical solution presented is valid for a cylindrical tube or thin disk with a concentric hole, subjected to internal and/or external pressure and a general radial temperature distribution. A specific problem examined is that of a thick walled cylinder subjected to an internal and external pressure loading and a linear radial temperature distribution. The results are expressed in nondimensional form and the effects on the response behavior are examined for various material properties, fiber orientation and types of loadings.

## INTRODUCTION

Recently, a continuum theory was presented for representing the thermoelastic behavior of unidirectional composites which can be idealized as a locally transverse isotropic homogeneous continua [1]. Applicability of a continuum theory for predicting deformations of composite (textured) materials depends relatively upon characteristic structural dimensions, the severity of gradients (i.e. stress, temperature, etc.), and the relative scale and periodicity of the material's internal structure.

Here, application of this transversely isotropic theory is made to the plane strain problem of a thick walled cylindrical tube subjected to internal and external pressure and a radial temperature distribution. The corresponding problem of a thin disk (plane stress case) with a concentric hole is also considered. Motivation for selecting the thick walled cylinder problem for investigation was twofold. The first is that it provides a simple structure that can be solved analytically, thereby supplying a benchmark problem for structural analysis code verification. Secondly, the thrust chambers of reusable rocket engines, notably the NASA Space Shuttle main engine, and tubular composite test specimens may be geometrically idealized as such. This enables a qualitative examination of the effect of fiber reinforcement on the stress, strain and deformation distributions.

The present study will be confined to examining the effect of material properties, fiber orientation and type of loading (in a general non-dimensional setting) on the thermoelastic behavior of a cylinder so as to develop an intuition with regard to the effects of transverse isotropy. In particular four types of pressure loadings (i.e. interior only, exterior less than interior, uniform and exterior greater than interior) and three types of linear radial temperature profiles (i.e. inner surface hotter than outer, uniform, and outer surface hotter than inner) will be examined.

This study begins with a brief description of the thermoelastic transversely isotropic constitutive theory and its plane strain and plane stress simplification. Next the analytical solution is presented in general form and then in a normalized form for a specific linear radial temperature distribution. A limited parametric study is then presented.

## CONSTITUTIVE EQUATIONS

Given a linear hyperelastic material reinforced by a single family of fibers the stress and strain components can be related through a normality structure utilizing a complementary energy function  $\Omega(\sigma_{ij}, d_i d_j, T)$ , i.e.

$$\epsilon_{ij} = \frac{\partial \Omega}{\partial \sigma_{ij}} \quad (1)$$

Here  $\sigma_{ij}$  denotes the components of (Cauchy) stress,  $\epsilon_{ij}$  the components of infinitesimal strain and the symmetric tensor  $d_i d_j$  is formed by a self product of the unit vector  $d_i$ , which denotes the local fiber direction and  $T$  represents temperature.

As discussed in [1] the complementary energy function may be expressed as:

$$\begin{aligned} \Omega(\sigma_{ij}, d_i d_j) &= A P_1 + B P_2 + C P_3 + D P_4 + E P_5 \\ &\quad + (F I_1 + H I_4) \Delta T \end{aligned} \quad (2)$$

where

$$P_1 = I_1^2$$

$$P_2 = I_2 - I_5 + \frac{1}{4} (I_4^2 - 9I_1^2 + 6I_1 I_4)$$

$$P_3 = I_5 - I_4^2 \quad (3)$$

$$P_4 = I_4^2$$

$$P_5 = I_1 I_4$$

and

$$I_1 = \sigma_{ii}/3$$

$$I_2 = \frac{1}{2} \sigma_{ij} \sigma_{ji}$$

$$I_4 = d_i d_j \sigma_{ji}$$

$$I_5 = d_i d_j \sigma_{jk} \sigma_{ki}$$

(4)

Note that in this report, the complementary energy function of equation (2) has been extended to include the effect of temperature.

Substituting equations (2) – (4) into equations (1) and associating coefficients A,B,C,D,E,F and H with physically measurable parameters (e.g. Young's modulus and Poisson ratio) as specified in [1] results in the following linear thermoelastic stress strain relations.

$$\begin{aligned} \epsilon_{ij} = & \left\{ -\frac{3\nu_T}{E_T} I_1 + \left( \frac{\nu_T}{E_T} - \frac{\nu_L}{E_L} \right) I_4 + a_T \Delta T \right\} \delta_{ij} \\ & + \left\{ 3 \left( \frac{\nu_T}{E_T} - \frac{\nu_L}{E_L} \right) I_1 + \left[ \frac{1+2\nu_L}{E_L} + \frac{1}{E_T} - \frac{1}{G_L} \right] I_4 + (a_L - a_T) \Delta T \right\} d_i d_j \\ & + \frac{1+\nu_T}{E_T} \sigma_{ij} + \left( \frac{1}{2G_L} - \frac{1+\nu_T}{E_T} \right) a_{ij} \end{aligned} \quad (5)$$

where

$\delta_{ij}$  – denotes the Kronecker delta function

$$a_{ij} = d_i \sigma_{jk} d_k + d_k \sigma_{ki} d_j$$

and

$G_T$  – Shear modulus (transverse) in the plane of isotropy

$G_L$  – Shear modulus (longitudinal) in a plane normal to the plane of isotropy.

$E_T$  – Young's modulus (transverse) in the plane of isotropy.

$E_L$  – Young's modulus (longitudinal) normal to the plane of isotropy.

$\nu_T$  – Poisson's ratio (transverse) that characterizes the transverse strain reduction in the plane of isotropy due to a tensile stress in the same plane.

$\nu_L$  – Poisson's ratio (longitudinal) that characterizes the transverse strain reduction in the plane of isotropy due to a tensile stress in a direction normal to it.

$\alpha_L$  – characterizes the thermal expansion normal to the plane of isotropy

$\alpha_T$  – characterizes the thermal expansion in the plane of isotropy

$\Delta T = T_2 - T_1$ ;  $T_1, T_2$  are two distinct temperatures.

## TWO DIMENSIONAL SIMPLIFICATION

Simplification of the multiaxial linear thermoelastic stress – strain relations of (5), is made to that of plane stress and plane strain. Out of the plane of isotropy (see figure 1), the plane stress assumption requires that the stress traction

$$\Gamma_i = \sigma_{ij} n_j = 0 \quad (6)$$

while plane strain requires

$$\epsilon_{11} = 0 \quad (7)$$

provided the local fiber direction ( $d_1$ ) and  $n_j$  (indicating the directionality of the plane stress or strain assumption) are defined as,

$$\begin{aligned}
d_1 &= \cos \varphi & n_1 &= 1 \\
d_2 &= \sin \varphi & n_2 &= 0 \\
d_3 &= 0 & n_3 &= 0
\end{aligned} \tag{8}$$

Note that the shear strain  $\epsilon_{12}$  is in general considered to be nonzero, while  $\epsilon_{13}$  would have been required to be equal to zero, if  $d_3$  had been nonzero. Given the above assumptions the following expressions relating the nonzero stress and strain components are obtained.

Plane Stress:

$$\begin{aligned}
\epsilon_r &= \sigma_r/E_T + \{-\nu_T/E_T + [\nu_T/E_T - \nu_L/E_L]s^2\} \sigma_\theta \\
&\quad + \alpha_T \Delta T
\end{aligned} \tag{9}$$

$$\begin{aligned}
\epsilon_\theta &= \{1/E_T + [1/2G_L - 1/E_T - \nu_L/E_L]s^2 + \\
&\quad [1/E_T + (1+2\nu_L)/E_L - 1/G_L]s^4\} \sigma_\theta + \\
&\quad \{-\nu_T/E_T + (\nu_T/E_T - \nu_L/E_L)s^2\} \sigma_r + [\alpha_T + (\alpha_L - \alpha_T)s^2] \Delta T
\end{aligned} \tag{10}$$

$$\begin{aligned}
\epsilon_{z\theta} &= \{[1/2G_L - 1/E_T - \nu_L/E_L]cs + [1/E_T + (1+2\nu_L)/E_L - 1/G_L]cs^3\} \sigma_\theta \\
&\quad + \{(\nu_T/E_T - \nu_L/E_L)cs\} \sigma_r + [(\alpha_L - \alpha_T)cs] \Delta T
\end{aligned} \tag{11}$$

$$\begin{aligned}
\epsilon_z &= \{-\nu_L/E_L + [1/E_T + (1+2\nu_L)/E_L - 1/G_L]s^2c^2\} \sigma_\theta + \\
&\quad \{-\nu_T/E_T + (\nu_T/E_T - \nu_L/E_L)c^2\} \sigma_r + [\alpha_T + (\alpha_L - \alpha_T)c^2] \Delta T
\end{aligned} \tag{12}$$

Plane Strain:

$$\begin{aligned} \epsilon_r = & \sigma_r \{1/E_T - C^2/A\} + \{-\nu_T/E_T + [\nu_T/E_T - \nu_L/E_L]s^2 \\ & - CB/A\} \sigma_\theta + \{\alpha_T - CD/A\} \Delta T \end{aligned} \quad (13)$$

$$\begin{aligned} \epsilon_\theta = & \{1/E_T + [1/2G_L - 1/E_T - \nu_L/E_L]s^2 + \\ & [1/E_T + (1+2\nu_L)/E_L - 1/G_L]s^4 - B^2/A\} \sigma_\theta \\ & + \{-\nu_T/E_T + (\nu_T/E_T - \nu_L/E_L)s^2 - BC/A\} \sigma_r + \\ & [\alpha_T + (\alpha_L - \alpha_T)s^2 - BD/A] \Delta T \end{aligned} \quad (14)$$

$$\begin{aligned} \epsilon_{z\theta} = & \{[1/2G_L - 1/E_T - \nu_L/E_L](1-B/A)cs + \\ & [1/E_T + (1+2\nu_L)/E_L - 1/G_L](cs^3 - (B/A)c^3s)\} \sigma_\theta \\ & + \{(\nu_T/E_T - \nu_L/E_L)cs - C/A([1/2G_L - 1/E_T - \nu_L/E_L]cs \\ & + [1/E_T + (1+2\nu_L)/E_L - 1/G_L]c^3s)\} \sigma_r \\ & + [(\alpha_L - \alpha_T)cs - (D/A)\{[1/2G_L - 1/E_T - \nu_L/E_L]cs \\ & + [1/E_T + (1+2\nu_L)/E_L - 1/G_L]c^3s\}] \Delta T \end{aligned} \quad (15)$$

$$\sigma_z = -(B/A)\sigma_\theta - (C/A)\sigma_r - (D/A)\Delta T \quad (16)$$

where A,B,C and D are defined in Appendix A and

$$s^n = \sin^n \varphi$$

$$n = 1, 2, 3 \text{ and } 4$$

$$c^n = \cos^n \varphi.$$

## ANALYTICAL SOLUTION

The problem under consideration is the solution of a thick walled circular cylinder with end caps composed of a locally transversely isotropic material (unidirectional

composite) which is subjected to a uniform internal ( $P_i$ ) and/or external ( $P_o$ ) pressure and a radial temperature distribution, see fig 2. The inner and outer radii are denoted by  $a$  and  $b$ , respectively, while  $T_a$  and  $T_b$  denote the applied temperature along the inner and outer radii of the cylinder. Generally a cylinder is classified as being thick walled when the wall thickness exceeds the inner radius by more than approximately 10%, i.e.  $b-a \geq 0.1$  or  $\lambda = b/a \geq 1.1$ .

### General Solution

The governing equations for this axisymmetrical problem, are:

Equilibrium – neglecting body forces

$$\sigma_{\theta} = \frac{d}{dr} (r\sigma_r) \quad (17)$$

$$\int_a^b \sigma_z 2\pi r dr = -\pi (b^2 P_o - a^2 P_i)$$

Strain – Displacements:

$$\epsilon_r = \frac{du}{dr} \quad (18)$$

$$\epsilon_{\theta} = \frac{u}{r}$$

and

Compatibility:

$$\epsilon_r = \frac{d}{dr} (r\epsilon_{\theta}) \quad (19)$$

where

$\sigma_r, \sigma_\theta$  is the radial and tangential (hoop) stress  
respectively

$\epsilon_r, \epsilon_\theta$  is the radial and tangential (hoop) strain  
respectively

Substituting the appropriate stress–strain relations , equations (9–10) and (13–14) into equation (19), simplifying and applying equilibrium the following Euler–Cauchy equation, describing the radial stress, results:

$$\sigma_r = \beta \left( \frac{d}{dr} \left( r \frac{d}{dr} (r \sigma_r) \right) - Q(r) \right)$$

or

$$r^2 \frac{d^2 \sigma_r}{dr^2} + 3r \frac{d \sigma_r}{dr} + \left(1 - \frac{1}{\beta}\right) \sigma_r = Q(r) \quad (20)$$

Here  $\beta$  and  $Q(r)$  are dependent upon the constitutive equations employed, e.g. plane stress or plane strain assumption (see Appendix A). Implied in equation (20) is the assumption that the material parameters (i.e.  $E_L, E_T, \nu_L, \nu_T, G_L, \alpha_L$  and  $\alpha_T$ ) are not strongly temperature dependent and therefore can be taken to be independent of radial location. Inclusion of this temperature dependence would only contribute higher order effects in the solution and distract attention from the primary emphasis of examining the effect of anisotropic coefficients of thermal expansion.

The general solution of (20) is

$$\sigma_r = C_1 r^{m_1} + C_2 r^{m_2} + Q_1(r) - Q_2(r) \quad (21)$$

where

$$Q_1(r) = \frac{r^{m_1}}{m_1 - m_2} \int r^{-(m_1+1)} Q(r) dr$$

$$Q_2(r) = \frac{r^{m_2}}{m_1 - m_2} \int r^{-(m_2+1)} Q(r) dr$$

$$m_1 = -1 + \Sigma$$

$$m_2 = -1 - \Sigma$$

$$\Sigma = \left| \sqrt{\frac{1}{\beta}} \right|$$

and as  $\beta$  is always positive, the roots ( $m_1$  and  $m_2$ ) are therefore real and distinct. The general solution for the tangential stress is obtained by substituting equation (21) into (17);

$$\begin{aligned} \sigma_{\theta} = C_1(m_1+1) r^{m_1} + C_2(m_2+1) r^{m_2} + (m_1+1) Q_1(r) \\ - (m_2+1) Q_2(r) \end{aligned} \quad (22)$$

The constants  $C_1$  and  $C_2$  are found by applying the boundary conditions:

$$(\sigma_r)_{r=a} = -P_i$$

$$(\sigma_r)_{r=b} = -P_o$$

to equation (21). The resulting expressions are

$$C_1 = \frac{a^{-m_2} P_i - b^{-m_2} P_o}{(b^{m_1 - m_2} - a^{m_1 - m_2})} + \frac{a^{-m_2} S(a) - b^{-m_2} S(b)}{(b^{m_1 - m_2} - a^{m_1 - m_2})} \quad (23)$$

$$C_2 = \frac{b^{-m_2} a^{m_1 - m_2} P_o - a^{-m_2} b^{m_1 - m_2} P_i}{(b^{m_1 - m_2} - a^{m_1 - m_2})} + \frac{a^{m_1 - m_2} b^{-m_2} S(b) - a^{-m_2} b^{m_1 - m_2} S(a)}{(b^{m_1 - m_2} - a^{m_1 - m_2})}$$

where  $S(r) = Q_1(r) - Q_2(r)$ .

Substituting  $C_1$  and  $C_2$  into equations (21) and (22) yield the following expressions representing  $\sigma_r$  and  $\sigma_\theta$  for either the plane stress or plane strain assumption and an arbitrary radial temperature distribution.

$$\begin{aligned} \sigma_r = & \left[ \frac{a^{-m_2} P_i - b^{-m_2} P_o}{(b^{m_1 - m_2} - a^{m_1 - m_2})} r^{m_1} + \frac{[b^{-m_2} a^{m_1 - m_2} P_o - a^{-m_2} b^{m_1 - m_2} P_i] r^{m_2} + \left[ \frac{\{a^{-m_2} Q_1(a) - b^{-m_2} Q_1(b)\} r^{m_1}}{(b^{m_1 - m_2} - a^{m_1 - m_2})} + \frac{\{a^{m_1 - m_2} b^{-m_2} Q_1(b) - a^{-m_2} b^{m_1 - m_2} Q_1(a)\} r^{m_2}}{(b^{m_1 - m_2} - a^{m_1 - m_2})} + Q_1(r) \right]}{(b^{m_1 - m_2} - a^{m_1 - m_2})} \right. \\ & \left. + \left[ - \frac{\{a^{-m_2} Q_2(a) - b^{-m_2} Q_2(b)\} r^{m_1}}{(b^{m_1 - m_2} - a^{m_1 - m_2})} - \frac{\{a^{m_1 - m_2} b^{-m_2} Q_2(b) - a^{-m_2} b^{m_1 - m_2} Q_2(a)\} r^{m_2}}{(b^{m_1 - m_2} - a^{m_1 - m_2})} - Q_2(r) \right] \right] \quad (24) \end{aligned}$$

$$\begin{aligned}
\sigma_{\theta} = & \frac{(m_1+1) \{ a^{-m_2} P_i - b^{-m_2} P_o \} r^{m_1}}{(b^{m_1-m_2} - a^{m_1-m_2})} + \\
& \frac{(m_2+1) \{ b^{-m_2} a^{m_1-m_2} P_o - a^{-m_2} b^{m_1-m_2} P_i \} r^{m_2}}{(b^{m_1-m_2} - a^{m_1-m_2})} + \\
& \left[ \frac{\{ a^{-m_2} Q_1(a) - b^{-m_2} Q_1(b) \} r^{m_1}}{(b^{m_1-m_2} - a^{m_1-m_2})} + \frac{\{ a^{m_1-m_2} b^{-m_2} Q_1(b) - a^{-m_2} b^{m_1-m_2} Q_1(a) \} r^{m_2}}{(b^{m_1-m_2} - a^{m_1-m_2})} \right. \\
& \left. + Q_1(r) \right] (m_1+1) + \\
& \left[ - \frac{\{ a^{-m_2} Q_2(a) - b^{-m_2} Q_2(b) \} r^{m_1}}{(b^{m_1-m_2} - a^{m_1-m_2})} - \frac{\{ a^{m_1-m_2} b^{-m_2} Q_2(b) - a^{-m_2} b^{m_1-m_2} Q_2(a) \} r^{m_2}}{(b^{m_1-m_2} - a^{m_1-m_2})} \right. \\
& \left. - Q_2(r) \right] (m_2+1) \tag{25}
\end{aligned}$$

If a linear radial temperature distribution is assumed

$$\Delta T = T_a - T_o + \frac{(T_b - T_a)}{(b - a)} (r - a)$$

and the resulting radial and tangential stress are non-dimensionalized, then the following expressions are obtained:

$$\begin{aligned}
\hat{\sigma}_r &= \frac{[1 - P\lambda^{1+\Sigma}]}{(\lambda^{2\Sigma} - 1)} \rho^{\Sigma-1} + \frac{[P\lambda^{1+\Sigma} - \lambda^{2\Sigma}]}{\lambda^{2\Sigma} - 1} \rho^{-(1+\Sigma)} \\
&+ \left[ 1 - \frac{\{\lambda^{1+\Sigma} - 1\}}{\{\lambda^{2\Sigma} - 1\}} \rho^{\Sigma-1} + \frac{\{\lambda^{1+\Sigma} - \lambda^{2\Sigma}\}}{\{\lambda^{2\Sigma} - 1\}} \rho^{-(1+\Sigma)} \right] Z_0 \\
&+ \left[ \rho - \frac{\{\lambda^{2+\Sigma} - 1\}}{\{\lambda^{2\Sigma} - 1\}} \rho^{\Sigma-1} + \frac{\{\lambda^{2+\Sigma} - \lambda^{2\Sigma}\}}{\{\lambda^{2\Sigma} - 1\}} \rho^{-(1+\Sigma)} \right] Z_1
\end{aligned} \tag{26}$$

$$\begin{aligned}
\hat{\sigma}_\theta &= \Sigma \frac{[1 - P\lambda^{1+\Sigma}]}{(\lambda^{2\Sigma} - 1)} \rho^{\Sigma-1} - \Sigma \frac{[P\lambda^{1+\Sigma} - \lambda^{2\Sigma}]}{\lambda^{2\Sigma} - 1} \rho^{-(1+\Sigma)} \\
&+ \left[ 1 - \Sigma \frac{\{\lambda^{1+\Sigma} - 1\}}{\{\lambda^{2\Sigma} - 1\}} \rho^{\Sigma-1} - \Sigma \frac{\{\lambda^{1+\Sigma} - \lambda^{2\Sigma}\}}{\{\lambda^{2\Sigma} - 1\}} \rho^{-(1+\Sigma)} \right] Z_0 \\
&+ \left[ 2\rho - \Sigma \frac{\{\lambda^{2+\Sigma} - 1\}}{\{\lambda^{2\Sigma} - 1\}} \rho^{\Sigma-1} - \Sigma \frac{\{\lambda^{2+\Sigma} - \lambda^{2\Sigma}\}}{\{\lambda^{2\Sigma} - 1\}} \rho^{-(1+\Sigma)} \right] Z_1
\end{aligned} \tag{27}$$

where

$$P = \frac{P_0}{P_i} \quad \hat{\sigma}_r = \frac{\sigma_r}{P_i}$$

$$\rho = \frac{r}{a}$$

$$\lambda = \frac{b}{a} \quad \hat{\sigma}_\theta = \frac{\sigma_\theta}{P_i}$$

Note  $\Sigma$ ,  $Z_0$  and  $Z_1$  are given in Appendix B for the plane stress and plane strain case. Neglecting all temperature dependence, the above equations can be shown to agree with the work of Lekhnitskii [2]

Knowing the non-dimensional radial and tangential stress components, the non-dimensional radial deformation, shear strain and either the longitudinal strain or stress components can be determined utilizing equations (6), (7),(18),(26) and (27).

The resulting expressions are:

$$\eta = \frac{u}{a} = \rho \left[ \frac{P_i}{E_T} \{ Z_2(\hat{\sigma}_r) + Z_3(\hat{\sigma}_\theta) \} + Z_4 \alpha_T \Delta T \right] \quad (28)$$

$$\hat{\epsilon}_{z\theta} = \frac{E_T \epsilon_{z\theta}}{P_i} = Z_5(\hat{\sigma}_r) + Z_6(\hat{\sigma}_\theta) + Z_7 \left( \frac{\alpha_T \Delta T E_T}{P_i} \right) \quad (29)$$

and for the plane stress assumption

$$\hat{\epsilon}_z = \frac{E_T \epsilon_z}{P_i} = Z_8(\hat{\sigma}_r) + Z_9(\hat{\sigma}_\theta) + Z_{10} \left( \frac{\alpha_T \Delta T E_T}{P_i} \right) \quad (30)$$

or plane strain assumption

$$\hat{\sigma}_z = \frac{\sigma_z}{P_i} = -\frac{C}{A}(\hat{\sigma}_r) - \frac{B}{A}(\hat{\sigma}_\theta) - \frac{D}{A} \left( \frac{\alpha_T \Delta T}{P_i} \right) \quad (31)$$

where

$$\Delta T = T_a \left\{ (1-\hat{T}) + \frac{(T-1)}{(\lambda-1)} (\rho-1) \right\}$$

and

$$\begin{aligned} T &= T_b/T_a \\ \hat{T} &= T_o/T_a \end{aligned}$$

and  $A, B, C, D, Z_2, Z_3, Z_4, Z_5, Z_6, Z_7, Z_8, Z_9,$  and  $Z_{10}$  are defined in Appendix B.

### Isotropic Simplification

Under isotropic conditions (i.e.  $E=E_L=E_T$ ,  $G=G_L=G_T$ ,  $\nu=\nu_L=\nu_T$  and  $\alpha=\alpha_L=\alpha_T$ ) the above plane strain expressions simplify to the following, which agree with solutions found in Timoshenko [2].

$$\begin{aligned} \hat{\sigma}_r &= \frac{[1-P\lambda^2]}{(\lambda^2-1)} + \frac{[P-1]}{\lambda^2-1} \frac{\lambda^2}{\rho^2} \\ &\quad - \left[ \rho - \frac{\{\lambda^3-1\}}{\{\lambda^2-1\}} + \frac{\lambda^2}{\{\lambda+1\}} \frac{1}{\rho^2} \right] \left[ \frac{EaT_a}{P_i} \frac{(T-1)}{(\lambda-1)} \frac{(1+\nu)}{3(1-\nu^2)} \right] \end{aligned} \quad (32)$$

$$\begin{aligned} \hat{\sigma}_\theta &= \frac{[1-P\lambda^2]}{(\lambda^2-1)} - \frac{[P-1]}{\lambda^2-1} \frac{\lambda^2}{\rho^2} \\ &\quad - \left[ 2\rho - \frac{\{\lambda^3-1\}}{\{\lambda^2-1\}} - \frac{\lambda^2}{\{\lambda+1\}} \frac{1}{\rho^2} \right] \left[ \frac{EaT_a}{P_i} \frac{(T-1)}{(\lambda-1)} \frac{(1+\nu)}{3(1-\nu^2)} \right] \end{aligned} \quad (33)$$

$$\eta = \rho \left[ \frac{P_i}{E} \{ (1-\nu^2) (\hat{\sigma}_\theta) - \nu(1+\nu) (\hat{\sigma}_r) \} + (1+\nu) a \Delta T \right] \quad (34)$$

$$\hat{\epsilon}_{z\theta} = 0 \quad (35)$$

$$\hat{\sigma}_z = \nu \left[ (\hat{\sigma}_r) + (\hat{\sigma}_\theta) \right] - \frac{(Ea \Delta T)}{P_i} \quad (36)$$

and  $P, \lambda, \rho, T$  and  $\Delta T$  are defined as before.

## DISCUSSION AND RESULTS

Comparing, in analytical form, the transversely isotropic solution, equations (26)–(31), to their isotropic counterparts equations (32)–(36), the following general observations can be made as to the significant role this special anisotropy plays.

- 1) The shear strain  $\epsilon_{z\theta}$  (eq. 29) is present for an arbitrary angle  $\varphi$ , however when the material is isotropic or the preferred direction is along the axis of symmetry ( $\varphi=0^\circ$ ) or perpendicular ( $\varphi=90^\circ$ ) no shear strain is computed.
- 2) The radial and tangential stress distribution is at most a function of  $(1/\rho^2)$  and  $\lambda^2$  for an isotropic material, whereas with an anisotropic material dependence on  $\rho$  and  $\lambda$  is now a function of material properties and angle of orientation.
- 3) In an isotropic material the longitudinal stress ( $\hat{\sigma}_z$ ) is independent of radial location ( $\rho$ ) and equal to a constant when only mechanical loads are present. Conversely when the material is anisotropic  $\hat{\sigma}_z$  is dependent upon material properties, angle of orientation and  $\rho$ . A similar statement can be made about the longitudinal strain ( $\epsilon_z$ ) when the plane stress assumption is invoked.

- 4) Considering only thermal loading, no stress is developed under a uniform temperature field if the material is isotropic. However stresses are developed in an anisotropic material provided the angle of orientation is not parallel with the axis of symmetry ( $\varphi=0^0$ ).

Note similar statements are applicable concerning items 1,2 and 4 when the plane stress assumption is invoked.

To gain a better understanding of the role anisotropy plays with regard to the stress distribution; various loading conditions, material parameters and fiber orientations will be considered. The presentation will be divided into three parts, i) internal/external pressure loading, ii) thermal loading and iii) thermomechanical loading. All results are presented in non-dimensional form.

#### Pressure Loading:

Considering only the application of internal and external pressure, equations (26) and (27) reduce to the following:

$$\hat{\sigma}_r = \frac{[1-P\lambda^{1+\Sigma}]}{(\lambda^{2\Sigma}-1)} \rho^{\Sigma-1} + \frac{[P\lambda^{1+\Sigma} - \lambda^{2\Sigma}]}{\lambda^{2\Sigma} - 1} \rho^{-(1+\Sigma)} \quad (37)$$

$$\hat{\sigma}_\theta = \Sigma \frac{[1-P\lambda^{1+\Sigma}]}{(\lambda^{2\Sigma}-1)} \rho^{\Sigma-1} - \Sigma \frac{[P\lambda^{1+\Sigma} - \lambda^{2\Sigma}]}{\lambda^{2\Sigma} - 1} \rho^{-(1+\Sigma)} \quad (38)$$

Taking the derivative of the normalized radial and tangential stress with respect to the normalized radius ( $\rho$ ) and equating them to zero allows one to obtain critical points where the stress distribution would remain stationary. The critical location for the radial stress is

$$\rho_{cr} = \left[ \frac{(1+\Sigma)(P\lambda^{1+\Sigma} - \lambda^{2\Sigma})}{(\Sigma-1)(1-P\lambda^{1+\Sigma})} \right]^{\frac{1}{2\Sigma}} \quad (39)$$

and for the tangential stress

$$\rho_{cr} = \left[ -\frac{(1+\Sigma)(P\lambda^{1+\Sigma} - \lambda^{2\Sigma})}{(\Sigma-1)(1-P\lambda^{1+\Sigma})} \right]^{\frac{1}{2\Sigma}} \quad (40)$$

For  $\rho_{cr}$  to be within the cylinder or disk it must be positive valued and be within the limits  $1 \leq \rho_{cr} \leq \lambda$ . Clearly no realistic stationary point is available for the tangential stress. A realistic stationary point may, however exist for the radial stress distribution as indicated in (39) depending upon the material parameters, fiber orientation, thickness and pressure ratio.

Calculations were performed to illustrate the above dependency on a transversely isotropic material with the assumed base material parameters listed in Table 1, for four types of pressure loadings, i.e.;

- 1) Interior pressure only,  $P=0$
- 2) Exterior pressure less than interior,  $P<1$
- 3) Equal interior and exterior pressure,  $P=1$
- 4) Exterior pressure greater than interior,  $P>1$

in figures 3 through 6, respectively. These figures show the effect fiber orientation, i.e.  $\varphi=0, 30, 60$  and  $90^\circ$ , has on the normalized radial stress distribution for a thick walled cylinder (plane strain assumption), with ratio of outer to inner wall radius ( $\lambda$ ) of 5.0.

Observe that when  $\varphi=0^\circ$ , the fiber orientation is aligned parallel with the axis of symmetry or equivalently the material is isotropic, i.e.  $\Sigma=1$ , thus we find from (39) that  $\rho_{cr} = \infty$ , therefore no stationary points exist within the cylinder or disk. Thus the

maximum/minimum radial stress occurs either at the inner or outer surface, see equation (37);

$$\begin{aligned} &\text{if } \rho = 1 && \left[ \hat{\sigma}_r \right] = -1 \\ \text{and} & && \\ &\text{if } \rho = \lambda && \left[ \hat{\sigma}_r \right] = -P \end{aligned}$$

depending upon the values of the applied pressures. This is consistent with well known classical solutions [3,4].

For example in figures 3 ( $P=0$ ) and 4 ( $P<1$ ) the maximum stress occurs at the inner surface, while in figure 5 ( $P=1$ ) it is constant and in figure 6 ( $P>1$ ) the maximum stress occurs along the outer surface. Clearly the development of stationary points within the cylinder is dependent upon orientation and loading. Case in point is observed in figure 4, were for  $\varphi=60$  and  $90^\circ$  the radial stress actually becomes less than the applied exterior pressure, which utilizing isotropic intuition should be the minimum stress obtainable. Conversely, the maximum stress continues to remain either at the interior or exterior surface independent of orientation, as one might expect since the stress component is governed by boundary conditions, i.e. the type of loading. The corresponding tangential stress distribution is shown in figures 7–10 respectively, for  $P=0$ ,  $P<1$ ,  $P=1$  and  $P>1$  and as indicated by (40) no stationary points are observed regardless of fiber orientation.

Work with isotropic thick walled cylinders [4] has shown that when both internal and external pressure act simultaneously the location of the maximum tangential stress, be it along the inner or outer surfaces, is dependent upon both geometry and the ratio of external to internal pressure. This conclusion is supported by the present work, figures 7–10, with the additional dependency of material property and fiber orientation due to the anisotropy of the material. This is evident in the following equation which expresses the

ratio of tangential stress at the inner ( $\rho=1$ ) and outer ( $\rho=\lambda$ ) surfaces:

$$S = \frac{\sigma_{\theta} \text{ inner}}{\sigma_{\theta} \text{ outer}} = \frac{(1 + \lambda^{2\Sigma}) - 2P\lambda^{1+\Sigma}}{2\lambda^{\Sigma-1} - P(1 + \lambda^{2\Sigma})} \quad (41)$$

In Table 2, equation (41) is utilized to obtain the required pressure ratios which would produce the following four example tangential stress ratios;

- 1) uniform tangential stress ( $S=1$ )
- 2) equal and opposite ( $S=-1$ )
- 3) inner tangential stress zero, outer tangential stress maximum ( $S=0$ )
- 4)  $0 < S < 1$ , which insures maximum tangential stress at the outer surface and that the sign of  $\hat{\sigma}_{\theta}$  remains the same throughout.

The fact that the sign of the tangential stress, as well as other stress components, can change from tension to compression or vice versa is important and should be considered when the elastic or inelastic material behavior is different in tension and compression, e.g. concrete or ceramics, as premature failure may result.

An example of the variation of the longitudinal stress ( $\hat{\sigma}_z$ ) with radius depending upon fiber orientation is illustrated in figure 11 for the case of  $P=0.5$ . The associated normalized radial displacement is shown in figure 12. Figure 13 shows the distribution of shear strain,  $\hat{\epsilon}_{z\theta}$ , with angle orientation for the case when  $P=2.0$ . Note that for  $\varphi = 0$  and  $90^\circ$  the shear strain is zero.

#### Variation of Material Property:

Thus far the effect of loading and fiber orientation on the distribution of stress and displacement has been examined. The above equations also indicate, however that the strength of anisotropy (specific material properties) will affect this distribution and as the material properties in Table 1 were chosen arbitrarily, the effect of their variation will now

be examined. As indicated in [1] to ensure convexity of the complementary energy function certain restrictions must be imposed on the material parameters. These restrictions are restated in non-dimensional form in Table 3. Next the effect of changing  $\xi$ ,  $\kappa$  and  $\nu_L$  when  $\nu_T$  is held fixed at 0.3 is investigated.

Figures 14 through 19 illustrate the effect that changing material properties have on the radial and tangential stress distributions for the case when the exterior pressure is twice that of the interior (i.e.  $P=2.0$ ) and the fibers are oriented at  $\varphi=60^\circ$ . In each figure only one material parameter is varied, while the remaining are equal to those prescribed in Table 1. Figures 14 – 19 clearly indicate that varying  $\kappa$  has the most significant effect upon both the radial and tangential distribution (with regard to curvature and maximum/minimum values) while varying  $\xi$  has the least. This trend appears to be independent of the type of pressure loading.

#### Thermal Loading:

Now considering only thermal loading equations (26) and (27) reduce to

$$\hat{\sigma}_r = \left[ 1 - \frac{\{\lambda^{1+\Sigma}-1\}}{\{\lambda^{2\Sigma}-1\}} \rho^{\Sigma-1} + \frac{\{\lambda^{1+\Sigma}-\lambda^{2\Sigma}\}}{\{\lambda^{2\Sigma}-1\}} \rho^{-(1+\Sigma)} \right]_{Z_0} + \left[ \rho - \frac{\{\lambda^{2+\Sigma}-1\}}{\{\lambda^{2\Sigma}-1\}} \rho^{\Sigma-1} + \frac{\{\lambda^{2+\Sigma}-\lambda^{2\Sigma}\}}{\{\lambda^{2\Sigma}-1\}} \rho^{-(1+\Sigma)} \right]_{Z_1} \quad (42)$$

$$\hat{\sigma}_\theta = \left[ 1 - \Sigma \frac{\{\lambda^{1+\Sigma}-1\}}{\{\lambda^{2\Sigma}-1\}} \rho^{\Sigma-1} - \Sigma \frac{\{\lambda^{1+\Sigma}-\lambda^{2\Sigma}\}}{\{\lambda^{2\Sigma}-1\}} \rho^{-(1+\Sigma)} \right]_{Z_0} + \left[ 2\rho - \Sigma \frac{\{\lambda^{2+\Sigma}-1\}}{\{\lambda^{2\Sigma}-1\}} \rho^{\Sigma-1} - \Sigma \frac{\{\lambda^{2+\Sigma}-\lambda^{2\Sigma}\}}{\{\lambda^{2\Sigma}-1\}} \rho^{-(1+\Sigma)} \right]_{Z_1} \quad (43)$$

Again taking the first derivative of the normalized radial and tangential stress with respect to the normalized radius ( $\rho$ ) and equating them to zero provides a condition to determine the critical location for the radial stress, i.e.

$$\begin{aligned}
& Z_1 - \frac{(\Sigma-1)}{(\lambda^{2\Sigma-1})} [Z_0\lambda^{1+\Sigma} + Z_1\lambda^{2+\Sigma} - (Z_0 + Z_1)] \rho^{\Sigma-2} \\
& - \frac{(\Sigma+1)}{(\lambda^{2\Sigma-1})} [Z_0\lambda^{1+\Sigma} + Z_1\lambda^{2+\Sigma} - (Z_0 + Z_1)\lambda^{2\Sigma}] \rho^{-\Sigma-2} = 0
\end{aligned} \tag{44}$$

and tangential stress

$$\begin{aligned}
& 2Z_1 - \frac{\Sigma(\Sigma-1)}{(\lambda^{2\Sigma-1})} [Z_0\lambda^{1+\Sigma} + Z_1\lambda^{2+\Sigma} - (Z_0 + Z_1)] \rho^{\Sigma-2} \\
& - \frac{\Sigma(\Sigma+1)}{(\lambda^{2\Sigma-1})} [Z_0\lambda^{1+\Sigma} + Z_1\lambda^{2+\Sigma} - (Z_0 + Z_1)\lambda^{2\Sigma}] \rho^{-\Sigma-2} = 0
\end{aligned} \tag{45}$$

where  $Z_0$  and  $Z_1$  are defined in Appendix B, for the plane stress or plane strain assumptions. A general solution for  $\rho$  critical is not straight forward, although it is clear that  $\rho_{cr}$  depends upon geometry ( $\lambda$ ), material properties (e.g.  $\xi$ ,  $\kappa$ ,  $\nu_L$  and  $\hat{\alpha}$ ), angle orientation ( $\varphi$ ) and thermal load ( $T$  and  $\hat{T}$ ). Under isotropic conditions (i.e.  $\Sigma=1$ ,  $\hat{\alpha}=1$ ) and assuming plane strain, equations (44) and (45) yield

$$\rho = \sqrt[3]{\frac{2\lambda^2}{\lambda+1}} \tag{46}$$

$$\rho = \sqrt[3]{\frac{-\lambda^2}{\lambda+1}} \quad (47)$$

respectively. Clearly no stationary point exists for the tangential stress, as  $\rho$  would be imaginary. The radial stress may, however have a stationary point depending of course upon the ratio  $\lambda$ .

Calculations were performed to investigate the above dependency for the transversely isotropic base material of Table 1, when

- 1) inner surface is hotter than the outer surface ( $T < 1$ )
- 2) uniform temperature field ( $T = 1$ )
- 3) outer surface is hotter than the inner surface ( $T > 1$ ).

For simplicity the temperature at the inner surface ( $T_a$ ) is assumed to be equal to the reference temperature ( $T_o$ ), i.e.  $\hat{T} = 1$ , except for case 2 ( $T = 1$ ) as both  $Z_0$  and  $Z_1$  would be equal to zero and no temperature loading would exist if  $\hat{T} = 1$ .

Figures 20 –23 show the radial and tangential stress distributions through the thickness of the cylinder at  $30^\circ$  increments in fiber orientations, for thermal loadings of  $T < 1$  and  $T > 1$  respectively. Clearly the sign for both the maximum radial and tangential stress (be it tensile or compressive) is dictated by the type of loading (i.e.  $T < 1$  or  $T > 1$ ) for a fixed  $\hat{T}$ . Also the location of the maximum radial stress is now angle and material dependent since the radial stress at the inner and outer surface are zero. The maximum tangential stress occurs at the inner surface independent of angle and thermal loading.

The variation with radius for  $\hat{\sigma}_z$  and  $\hat{\epsilon}_{z\theta}$  are given in figures 24 and 25 for load case 1 ( $T < 1$ ). As one would expect  $\hat{\sigma}_z$  varies linearly with  $\rho$  at a  $0^\circ$  fiber orientation and the normalized shear strain ( $\hat{\epsilon}_{z\theta}$ ) is zero. A non-zero shear strain and a nonlinear distribution of  $\hat{\sigma}_z$  is observed for off-axis orientations and (as with pressure loadings) the magnitude is highly dependent upon material properties, thickness ( $\lambda$ ) and angle.

The radial stress distribution produced for a given fiber orientation under a uniform temperature ( $T=1$ ) distribution is shown in figure 26. No radial (or tangential) stress is calculated for a  $0^\circ$  orientation as one would expect since both  $\hat{\sigma}_r$  and  $\hat{\sigma}_\theta$  are in the plane of isotropy. Note that the sign (tensile or compressive) of the stress (radial or tangential) is dependent upon whether the applied thermal load is above ( $\hat{T}<1$ ) or below ( $\hat{T}>1$ ) the reference temperature. In figure 26,  $\hat{T}$  is equal to 0.5. It is important to realize that both expansion and contraction could take place within the thickness of the cylinder if both  $T$  and  $\hat{T}$  are less than or greater than one, but not equal.

#### Variation of Material Properties:

The effect of varying material property parameters, when the cylinder is subjected to a thermal load is very similar to that shown for the pressure loadings. For example in figures 27 and 28 the effect on the radial stress distribution of changing  $\xi$ , (i.e.  $\xi=2,5$  and  $10$ ) and  $\kappa$  (i.e.  $\kappa = 0.8,1.0,2.0$  and  $4.0$ ) are shown respectively for the case when  $T=0.5$ ,  $\hat{T} = 1.0$ ,  $\hat{\alpha}=0.5$  and at a fiber angle of  $60^\circ$ , see figure 20. In addition to varying these mechanical material parameters, the coefficient of thermal expansion will play a significant role in two ways.

The first is its effect on the sign of the stress; for example if  $\hat{\alpha}=\alpha_L/\alpha_T>1$  (cf. figure 26 where  $\hat{\alpha}=2.0$  and  $\hat{T}<1$ )  $\hat{\sigma}_r$  is tensile whereas if  $\hat{\alpha}<1$  (cf. figure 29 where  $\hat{\alpha}=0.5$  and  $\hat{T}<1$  and  $T=1$ )  $\hat{\sigma}_r$  is compressive. The second is in the actual magnitude and how it affects the magnitude of the various stress components as illustrated in figures 30 and 31 where  $\hat{\sigma}_r$  and  $\hat{\sigma}_\theta$  versus  $\rho$  are displayed respectively. For the case when  $T=2.0$ ,  $\hat{T}=1$ ,  $\varphi= 60^\circ$  and  $\hat{\alpha} = -0.25,0.0,0.25,0.5,1.0$  and  $2.0$ . Figure 30 and 31 clearly indicate that as  $\hat{\alpha}$  approaches zero a minimum radial and tangential stress state is reached. This  $\hat{\alpha}$  value, which produces a minimum stress state is not unique as it is highly fiber orientation dependent. Examples of this are shown in figures 32 and 33 for the identical case shown in figure 30 but with the angle  $\varphi$  being changed to  $30$  and  $90^\circ$  respectively.

It is important to realize that in a macroscopic sense the magnitude of  $\hat{\alpha} = \alpha_L / \alpha_T$  represents the ratio between the longitudinal and transverse coefficient of expansion or in an averaged sense the amount of  $\alpha$  mismatch there is between fiber and matrix assuming longitudinally aligned fibers. For example assume we have a cube of composite material subjected to a change in temperature. If the amount of elongation parallel and transverse to the fibers is the same then  $\alpha_L = \alpha_T$  and  $\hat{\alpha} = 1$ . Similarly an  $\hat{\alpha} = 1$  would be equivalent to no  $\alpha$  mismatch between the fiber and matrix provided that the coefficients of thermal expansion in all directions are equal [5]. The point is that elimination of any  $\alpha$  mismatch between fiber and matrix may not be the most desirable path to follow if one wishes to minimize the macro stress state within a structure. Therefore by selecting the appropriate system one might be able to optimize the  $\alpha$  mismatch for a particular structure, applied load(s) and fiber orientation. Clearly the implied assumption here is that the micro stresses developed due to this optimum  $\alpha$  mismatch are insufficient to cause self destruction of the material.

#### **Thermomechanical:**

Thermomechanical results can be obtained from the above results by superimposing the various pressure loadings on those of the pure thermal loading. Equations 26 – 31 are valid for any arbitrary pressure and/or linear temperature loading. The response behavior is highly dependent upon the given type of loading, material properties, fiber orientation and geometry. An example is shown in figures 34 and 35 where the normalized radial and tangential stress versus the normalized radius  $\rho$  are shown respectively when a uniform pressure loading (cf figures 5 and 9) is superimposed on a temperature profile whereby the outer surface is twice that of the inner (cf figures 22 and 23). One observes from figure 34 that the radial stress now changes sign from compressive to tensile stress and that the stress distribution is now relatively insensitive to fiber orientation. The insensitivity to

orientation is merely a coincidence as clearly shown in figure 36 where the temperature at the outer surface is now four times that of the inner.

## CONCLUSIONS:

A continuum theory representing the thermoelastic behavior of unidirectional composites has been applied to the problem of a thick walled cylindrical tube subjected to internal and external pressure and a radial temperature distribution. The resulting analytical solution was then specialized for a linear radial temperature distribution and was expressed in non-dimensional form. A limited parametric study was conducted in which four types of pressure loadings and three types of radial temperature profiles were examined to develop intuition with regard to the effects of transverse isotropy.

This analytical solution provides a benchmark problem for structural analysis code verification and may be employed to illustrate the stress, strain and deformation distributions within a unidirectional tubular composite test specimen or the thrust chambers of reusable rocket engines. The results clearly illustrate that the stress and strain response is highly dependent upon geometry, fiber orientation, material properties and type of loading. Finally it was illustrated that to minimize the macro stress or strain state within this structure subjected to the given pressure and thermal loadings a non unique  $\alpha$  mismatch would be desired. This mismatch is highly dependent upon fiber orientation, material property and geometry.

## REFERENCES

- 1) Arnold, S.M., "A Transversely Isotropic Thermoelastic Theory", NASA TM101302, Aug 1988.
- 2) Lekhnitskii, S.G., Theory of Elasticity of an Anisotropic Body, Holden-Day, San Francisco, pp. 44,45 and 249-252, 1963.

- 3) Timoshenko, S.P. and Goodier, J.N., Theory of Elasticity, McGraw-Hill, New York, pp 441–451, 1970.
- 4) Ugural, A.C. and Fenster, S.K., Advanced Strength and Applied Elasticity, Elsevier, New York, pp 246–253, 1975.
- 5) Hashin, Z., "Analysis of Composite Materials – A Survey", *Jnl. of Appl. Mech.*, Vol 50, pp 481–505, 1983.

## APPENDIX A

Material dependent parameters of the Euler–Cauchy Equation.

Plane Stress (utilizing equations (6))

$$\beta = E_T \left\{ \frac{1}{\bar{E}_T} + \left( \frac{1}{\bar{G}_L} - \frac{2}{\bar{E}_T} - \frac{2\nu_L}{\bar{E}_L} \right) s^2 + \left( \frac{1}{\bar{E}_T} + \frac{(1+2\nu_L)}{\bar{E}_L} - \frac{1}{\bar{G}_L} \right) s^4 \right\}$$

$$Q(r) = \frac{-E_T}{\beta} \left\{ (a_L - a_T) s^2 \Delta T + (a_T + (a_L - a_T) s^2) r \frac{d \Delta T}{dr} \right\}$$

Plane strain (utilizing equations (7))

$$\beta = \frac{\left\{ \frac{1}{\bar{E}_T} + \left( \frac{1}{\bar{G}_L} - \frac{2}{\bar{E}_T} - \frac{2\nu_L}{\bar{E}_L} \right) s^2 + \left( \frac{1}{\bar{E}_T} + \frac{(1+2\nu_L)}{\bar{E}_L} - \frac{1}{\bar{G}_L} \right) s^4 - \frac{B^2}{A} \right\}}{\left[ \frac{1}{\bar{E}_T} - \frac{C^2}{A} \right]}$$

$$Q(r) = \beta_1' \Delta T + \beta_2' r \frac{d \Delta T}{dr}$$

where

$$\beta_1' = \frac{-[(a_L - a_T) s^2 + (C - B) D]}{A} \left\{ \frac{1}{\bar{E}_T} + \left( \frac{1}{\bar{G}_L} - \frac{2}{\bar{E}_T} - \frac{2\nu_L}{\bar{E}_L} \right) s^2 + \left( \frac{1}{\bar{E}_T} + \frac{(1+2\nu_L)}{\bar{E}_L} - \frac{1}{\bar{G}_L} \right) s^4 - \frac{B^2}{A} \right\}$$

$$\beta_2' = \frac{-[a_T + (a_L - a_T)s^2 - \frac{BD}{A}]}{\left\{ \frac{1}{\bar{E}_T} + \left( \frac{1}{\bar{G}_L} - \frac{2}{\bar{E}_T} - \frac{2\nu_L}{\bar{E}_L} \right) s^2 + \left( \frac{1}{\bar{E}_T} + \frac{(1+2\nu_L)}{\bar{E}_L} - \frac{1}{\bar{G}_L} \right) s^4 - \frac{B^2}{A} \right\}}$$

and

$$A = \left\{ \frac{1}{\bar{E}_T} + \left( \frac{1}{\bar{G}_L} - \frac{2}{\bar{E}_T} - \frac{2\nu_L}{\bar{E}_L} \right) c^2 + \left( \frac{1}{\bar{E}_T} + \frac{(1+2\nu_L)}{\bar{E}_L} - \frac{1}{\bar{G}_L} \right) c^4 \right\}$$

$$B = \left\{ -\frac{\nu_L}{\bar{E}_L} + \left( \frac{1}{\bar{E}_T} + \frac{(1+2\nu_L)}{\bar{E}_L} - \frac{1}{\bar{G}_L} \right) s^2 c^2 \right\}$$

$$C = \left\{ -\frac{\nu_T}{\bar{E}_T} + \left( \frac{\nu_T}{\bar{E}_T} - \frac{\nu_L}{\bar{E}_L} \right) c^2 \right\}$$

$$D = [ a_T + (a_L - a_T)c^2 ]$$

$$\Delta T = T(r) - T_0$$

$$s^n = \sin^n \varphi \quad n = 2, 4$$

$$c^n = \cos^n \varphi$$

## APPENDIX B

### Non-dimensional material dependent coefficients

With the following defined quantities:

$$\kappa = \frac{E_T}{G_L} \qquad \hat{a} = \frac{a_L}{a_T} \qquad \hat{T} = \frac{T_o}{T_a}$$

$$\xi = \frac{E_L}{E_T} \qquad T = \frac{T_b}{T_a}$$

$$A = \left\{ 1 + \left( \kappa - 2 - \frac{2\nu_L}{\xi} \right) c^2 + \left( 1 - \kappa + \frac{(1+2\nu_L)}{\xi} \right) c^4 \right\}$$

$$B = \left\{ -\frac{\nu_L}{\xi} + \left( 1 + \frac{(1+2\nu_L)}{\xi} - \kappa \right) s^2 c^2 \right\}$$

$$C = \left\{ -\nu_T + \left( \nu_T - \frac{\nu_L}{\xi} \right) c^2 \right\}$$

$$D = [ 1 + (\hat{a} - 1) c^2 ]$$

$$s^n = \sin^n \varphi \qquad n = 1, 2, 3, 4$$

$$c^n = \cos^n \varphi$$

the non-dimensional material dependent coefficients for plane stress and strain assumption may be obtained.

Plane stress (utilizing equations (6))

$$\Sigma^2 = 1/\beta$$

$$\beta = \left\{ 1 + \left( \kappa - 2 - \frac{2\nu_L}{\xi} \right) s^2 + \left( 1 + \frac{(1+2\nu_L)}{\xi} - \kappa \right) s^4 \right\}$$

$$Z_0 = \frac{-E_T a_T T_a}{P_i(\beta - 1)} \left[ (\hat{a} - 1) s^2 \right] \left[ \frac{(\lambda - T) - \hat{T}}{(\lambda - 1)} \right]$$

$$Z_1 = \frac{-E_T a_T T_a}{P_i(4\beta - 1)} \left[ 1 + 2(\hat{a} - 1) s^2 \right] \frac{(T - 1)}{(\lambda - 1)}$$

$$Z_2 = \frac{(\nu_T - \nu_L) s^2 - \nu_T}{\xi}$$

$$Z_3 = \beta$$

$$Z_4 = 1 + (\hat{a} - 1) s^2$$

$$Z_5 = \frac{(\nu_T - \nu_L) c s}{\xi}$$

$$Z_6 = \left( \frac{K}{2} - 1 - \frac{\nu_L}{\xi} \right) c s + \left( 1 + \frac{(1+2\nu_L)}{\xi} - \kappa \right) c s^3$$

$$Z_7 = (\hat{a} - 1) c s$$

$$Z_8 = -\nu_T + (\nu_T - \frac{\nu_L}{\xi}) c^2$$

$$Z_9 = \frac{-\nu_L}{\xi} + \left( 1 + \frac{(1 + 2\nu_L)}{\xi} - \kappa \right) s^2 c^2$$

$$Z_{10} = 1 + (\hat{a} - 1) c^2$$

Plane strain (utilizing equations (7))

$$\Sigma^2 = [1 - \frac{c^2}{\lambda}] / \beta$$

$$\beta = \left\{ 1 + (\kappa - 2 - \frac{2\nu_L}{\xi})s^2 + (1 + \frac{(1+2\nu_L)}{\xi} - \kappa)s^4 - \frac{B^2}{\lambda} \right\}$$

$$Z_0 = \frac{-E_T a_T T_a}{P_i (\beta - 1 + c^2)} \frac{[(\hat{a} - 1)s^2 + (C - B)D]}{\lambda} \frac{[(\lambda - T) - \hat{T}]}{(\lambda - 1)}$$

$$Z_1 = \frac{-E_T a_T T_a}{P_i (4\beta - 1 + c^2)} \frac{[1 + 2(\hat{a} - 1)s^2 + (C - 2B)D]}{\lambda} \frac{(T - 1)}{(\lambda - 1)}$$

$$Z_2 = \frac{(\nu_T - \nu_L)s^2 - \nu_T - \frac{BC}{\lambda}}{\xi}$$

$$Z_3 = \beta$$

$$Z_4 = 1 + \frac{(\hat{a} - 1)s^2 - BD}{\lambda}$$

$$Z_5 = \frac{(\nu_T - \nu_L)cs - \frac{C}{D} \left\{ (\frac{K}{2} - 1 - \frac{\nu_L}{\xi})cs + (1 + \frac{(1+2\nu_L)}{\xi} - \kappa)c^3s \right\}}{\xi}$$

$$Z_6 = \left( \frac{K}{2} - 1 - \frac{\nu_L}{\xi} \right) cs \left( 1 - \frac{B}{\lambda} \right) + \left( 1 + \frac{(1+2\nu_L)}{\xi} - \kappa \right) (cs^3 - \frac{B}{\lambda} c^3s)$$

$$Z_7 = \frac{(\hat{a} - 1)cs - \frac{D}{\lambda} \left\{ (\frac{K}{2} - 1 - \frac{\nu_L}{\xi})cs + (1 + \frac{(1+2\nu_L)}{\xi} - \kappa)c^3s \right\}}{\xi}$$

TABLE 1  
Base Material Parameters

$E_T = 15000 \text{ ksi}$	
$\nu_L = 0.8$	$\xi = 5.0$
$\nu_T = 0.3$	$\kappa = 2.0$
$\alpha_T = 3.0 \times 10^{-6}$	$\hat{\alpha} = 0.5$

TABLE 2  
Required Pressure Ratio to Produce the Circumferential Stress Ratio

$S = -1$	$P = \frac{1 + \lambda^{2\Sigma} + 2\lambda^{\Sigma-1}}{1 + \lambda^{2\Sigma} + 2\lambda^{1+\Sigma}}$
$S = 0$	$P = \frac{1 + \lambda^{2\Sigma}}{2\lambda^{1+\Sigma}}$
$S = 1$	$P = \frac{2\lambda^{\Sigma-1} - 1 - \lambda^{2\Sigma}}{1 + \lambda^{2\Sigma} - 2\lambda^{1+\Sigma}}$
$0 < S < 1$	$\frac{1 + \lambda^{2\Sigma}}{2\lambda^{1+\Sigma}} < P < \frac{2\lambda^{\Sigma-1} - 1 - \lambda^{2\Sigma}}{1 + \lambda^{2\Sigma} - 2\lambda^{1+\Sigma}}$

**TABLE 3**  
**Inequalities Required to Maintain Convexity of Potential**

$$\xi > 0; \quad \xi > \nu_L^2; \quad \xi > \frac{2\nu_L}{1-\nu_T}; \quad \kappa \geq \frac{2(1+\nu_L)}{\xi}$$

$\xi$	$\frac{(1-\nu_T)\xi}{2} > \nu_L^2$	$\kappa \geq \frac{2(1+\nu_L)}{\xi}$
2.0	$0.836 > \nu_L$	$\kappa \geq 1.8$
5.0	$1.322 > \nu_L$	$\kappa \geq 0.72$
10.0	$1.87 > \nu_L$	$\kappa \geq 0.36$

## NOMENCLATURE

$\Omega$	– Complementary Energy Function
$d_i$	– Vector denoting local fiber direction
$\epsilon_{ij}$	– total infinitesimal strain tensor
$\sigma_{ij}$	– Cauchy stress tensor
$T$	– Temperature
$P_k$	– Physical Invariants $k=1,2,3,4,5$
$I_k$	– Invariants $k=1,2,4,5$
$G_T$	– Transverse shear modulus
$G_L$	– Longitudinal shear modulus
$E_T$	– Transverse Young's modulus
$E_L$	– Longitudinal Young's modulus
$\nu_T$	– Transverse poisson's ratio
$\nu_L$	– Longitudinal Poisson's ratio
$\alpha_L$	– Longitudinal thermal expansion
$\alpha_T$	– Transverse thermal expansion
$\hat{\alpha}$	– normalized thermal expansion coefficient, $\alpha_L/\alpha_T$
$\Gamma_i$	– Stress traction vector
$\varphi$	– Angle between axes 1 and 2 or z and $\theta$ .
$P_i$	– Internal pressure
$P_o$	– External pressure
$P$	– Normalized pressure, i.e $P_i/P_o$ .
$a$	– inner wall radius
$b$	– outer wall radius
$T_a$	– temperature at inner wall
$T_b$	– temperature at outer wall
$T$	– ratio of temperature of outer wall to that of inner.
$\lambda$	– ratio of outer wall radius to that of inner.
$u$	– radial displacement
$\eta$	– normalized radial displacement, $=u/a$
$r$	– radial location
$\rho$	– normalized radial location, $=r/a$
$\sigma_r, \epsilon_r$	– radial stress and strain component respectively.
$\sigma_\theta, \epsilon_\theta$	– tangential stress and strain component respectively.

$\sigma_z, \epsilon_z$  — longitudinal stress and strain component respectively

$\hat{\sigma}_r$  — normalized radial stress component.

$\hat{\sigma}_\theta$  — normalized tangential stress component.

$\hat{\sigma}_z$  — normalized longitudinal stress component.

$\hat{\epsilon}_z$  — normalized longitudinal strain component.

$\hat{\epsilon}_{z\theta}$  — normalized shear strain component.

$\hat{T}$  — normalized reference temperature,  $= T_0/T_a$

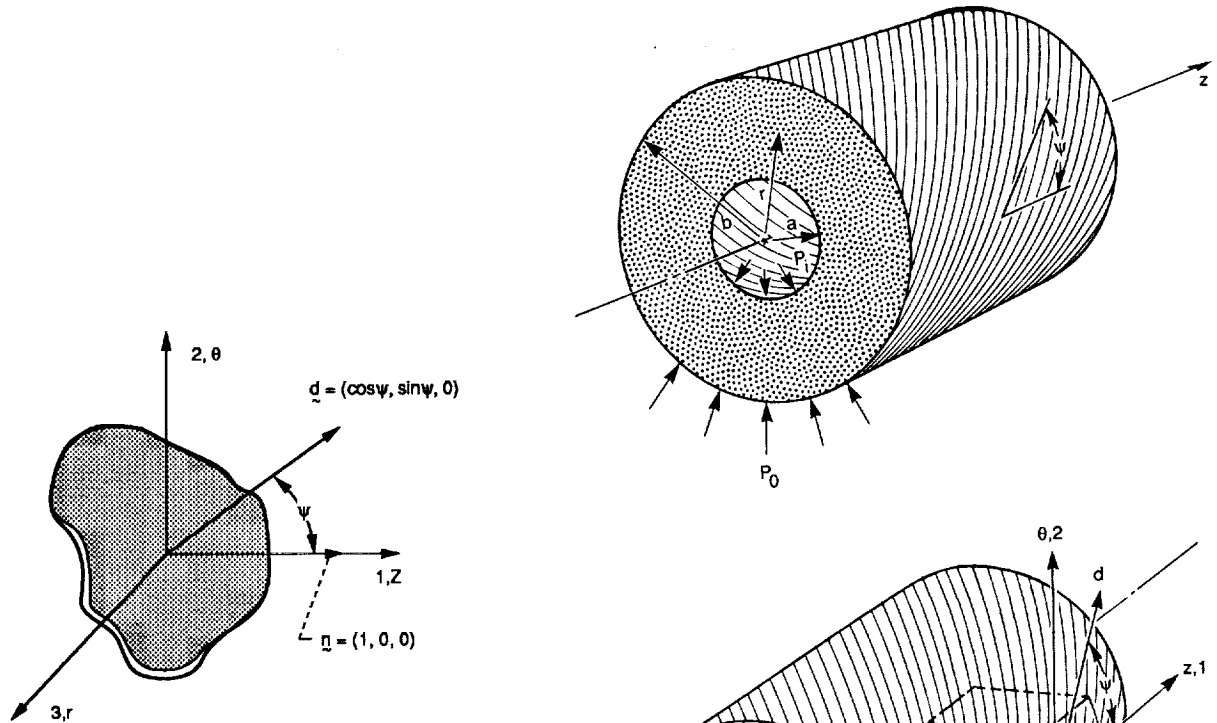


Figure 1. - Definition of coordinate system and plane of isotropy.

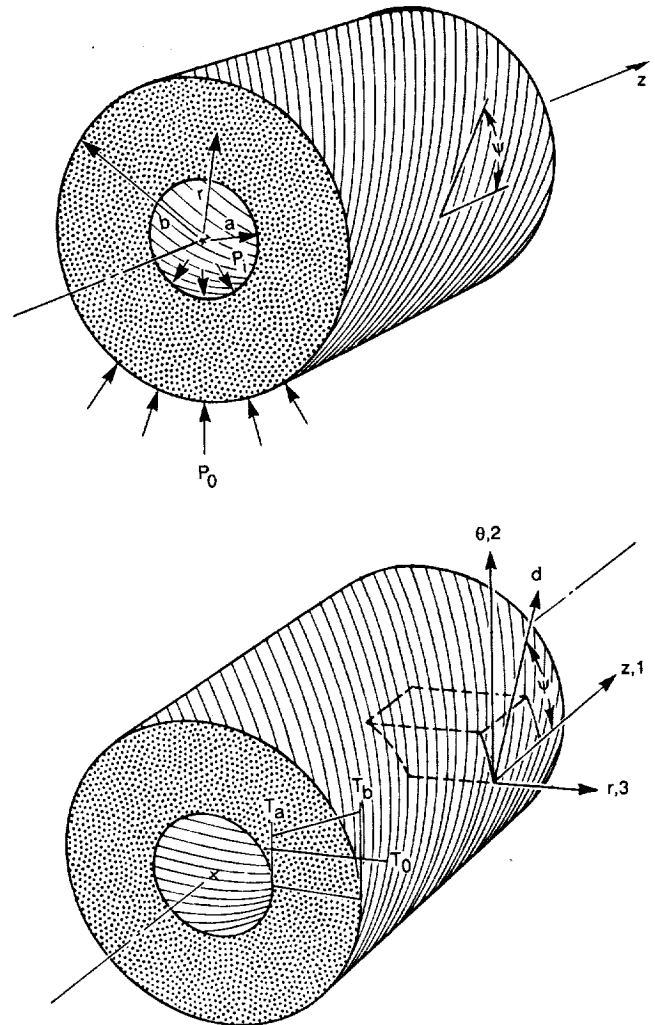


Figure 2. - Schematic of thick walled cylindrical composite.

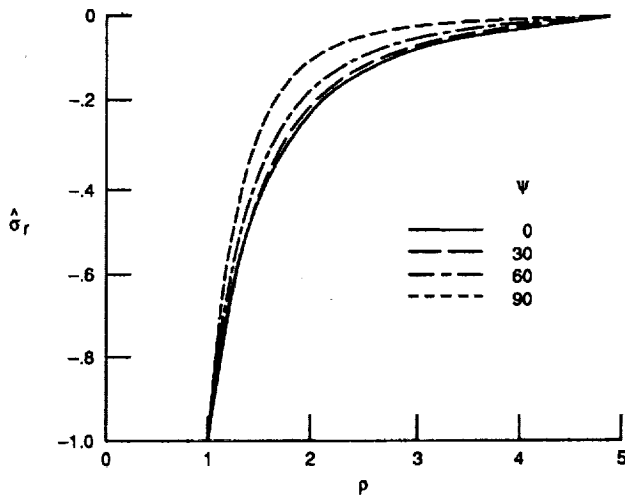


Figure 3. - Normalized radial stress versus normalized radius for fiber orientations of 0, 30, 60 and 90° and interior pressure only,  $P = 0$ .

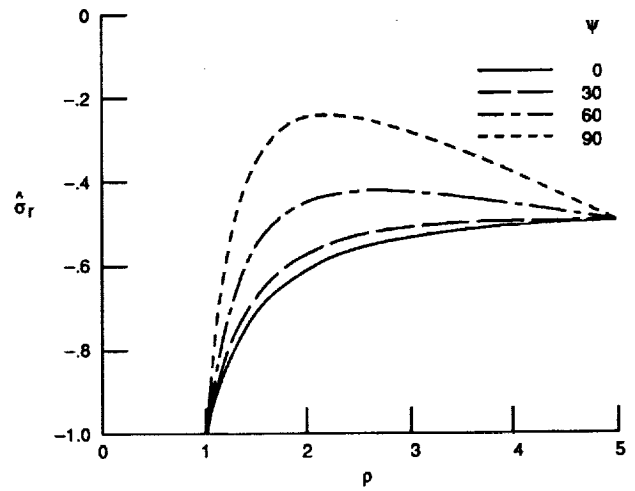


Figure 4. - Normalized radial stress versus normalized radius for fiber orientations of 0, 30, 60 and 90° and interior pressure greater than exterior,  $P = 0.5$ .

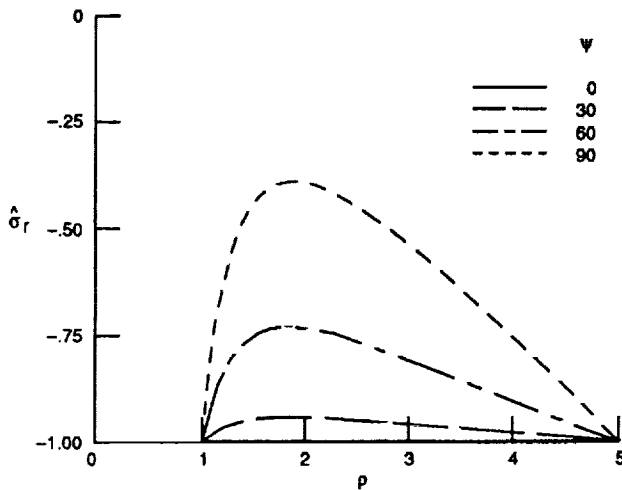


Figure 5. - Normalized radial stress versus normalized radius for fiber orientations of 0, 30, 60 and 90° and uniform pressure,  $P = 1$ .

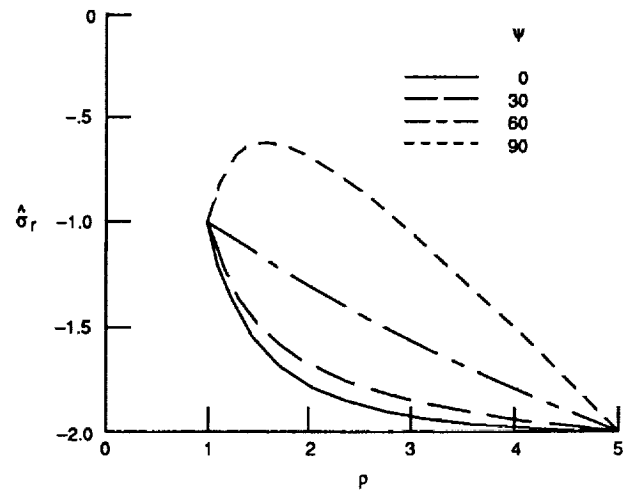


Figure 6. - Normalized radial stress versus normalized radius for fiber orientations of 0, 30, 60 and 90° and exterior pressure greater than interior,  $P = 2$ .

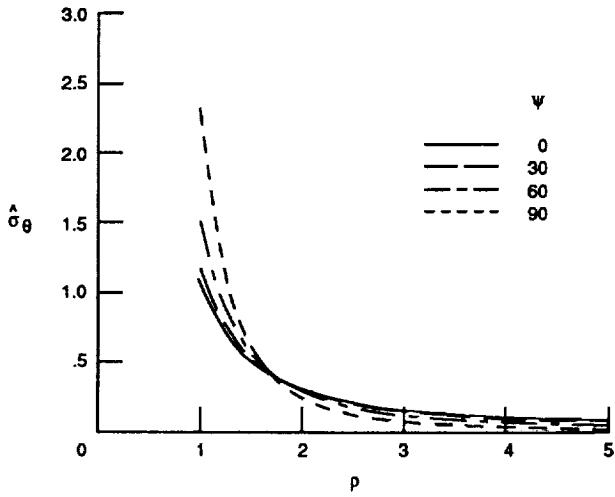


Figure 7. - Normalized tangential stress versus normalized radius for fiber orientations of 0, 30, 60 and 90° and interior pressure only,  $P = 0$ .

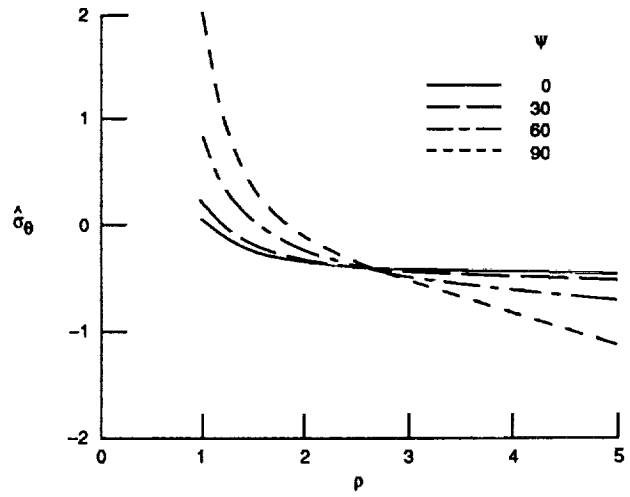


Figure 8. - Normalized tangential stress versus normalized radius for fiber orientations of 0, 30, 60 and 90° and interior pressure greater than exterior,  $P = 0.5$ .

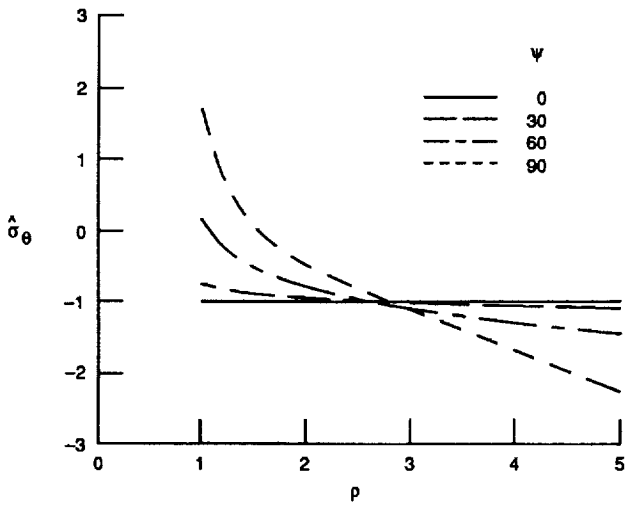


Figure 9. - Normalized tangential stress versus normalized radius for fiber orientations of 0, 30, 60 and 90° and uniform pressure,  $P = 1$ .

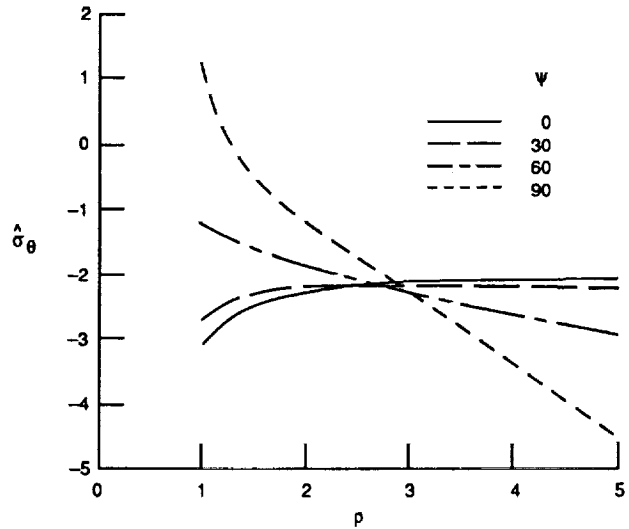


Figure 10. - Normalized tangential stress versus normalized radius for fiber orientations of 0, 30, 60 and 90° and exterior pressure greater than interior,  $P = 2$ .

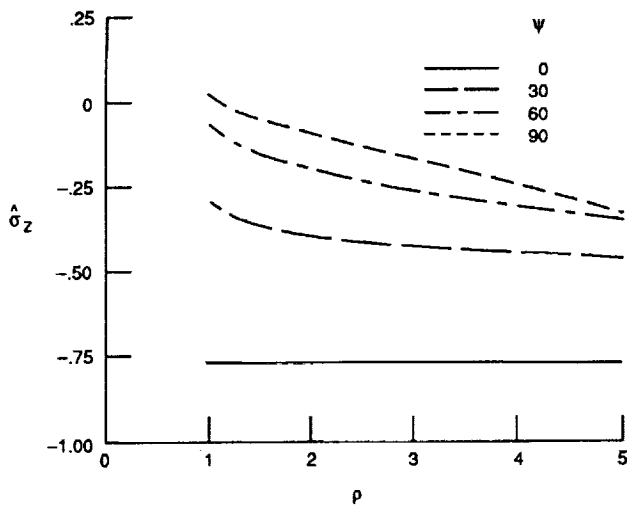


Figure 11. - Normalized longitudinal stress versus normalized radius for fiber orientations of 0, 30, 60 and 90° and interior pressure greater than exterior,  $P = 0.5$ .

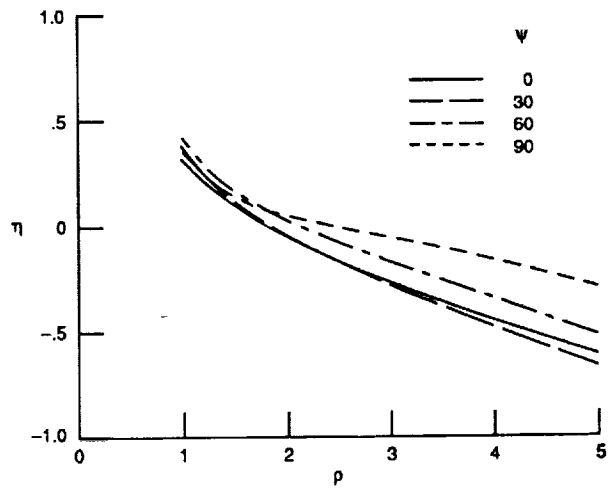


Figure 12. - Normalized radial displacement versus normalized radius for fiber orientations of 0, 30, 60 and 90° and interior pressure greater than exterior,  $P = 0.5$ .

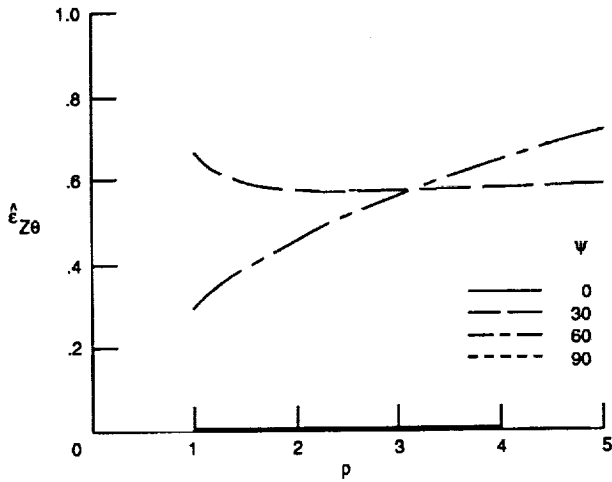


Figure 13. - Normalized shear strain versus normalized radius for fiber orientations of 0, 30, 60 and 90° and exterior pressure greater than interior,  $P = 2$ .

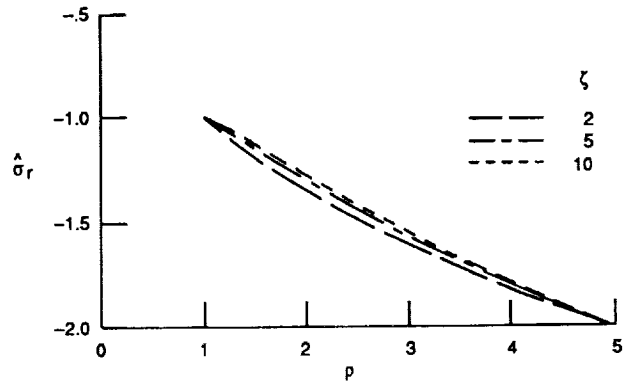


Figure 14. - Normalized radial stress versus normalized radius for varying  $\zeta$ , i.e., 2, 5, and 10 at fiber orientation of 60° and exterior pressure greater than interior,  $P = 2$ .

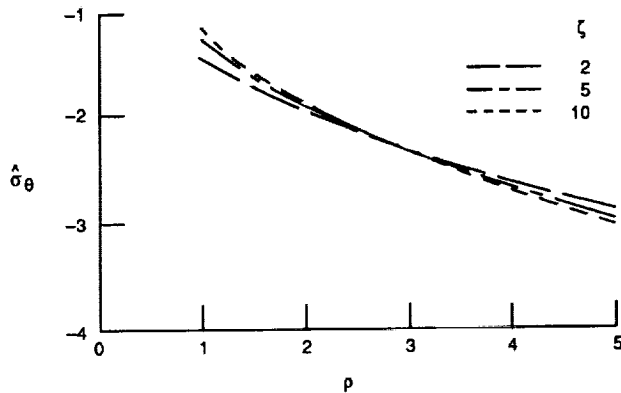


Figure 15. - Normalized tangential stress versus normalized radius for varying  $\zeta$ , i.e., 2, 5, and 10 at fiber orientation of 60° and exterior pressure greater than interior,  $P = 2$ .

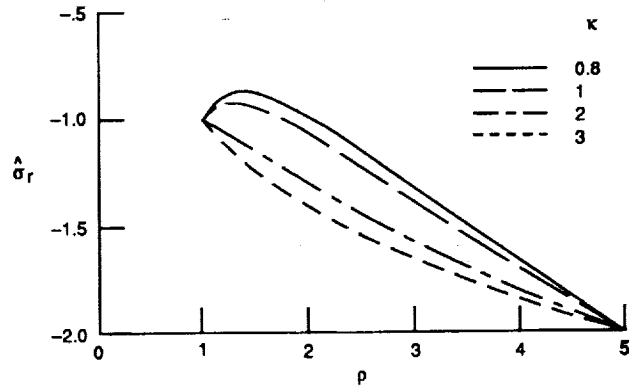


Figure 16. - Normalized radial stress versus normalized radius for varying  $\kappa$ , i.e., 0.8, 1.0, 2.0 and 3.0, at fiber orientation of 60° and exterior pressure greater than interior,  $P = 2$ .

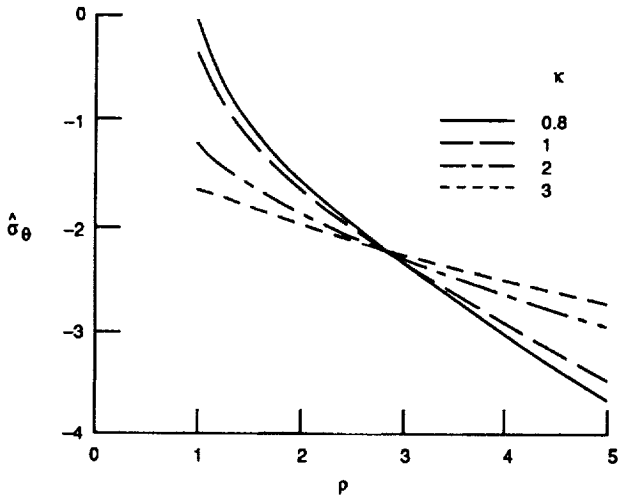


Figure 17. - Normalized tangential stress versus normalized radius for varying  $\kappa$ , i.e., 0.8, 1.0, 2.0 and 3.0, at fiber orientation of  $60^\circ$  and exterior pressure greater than interior,  $P = 2$ .

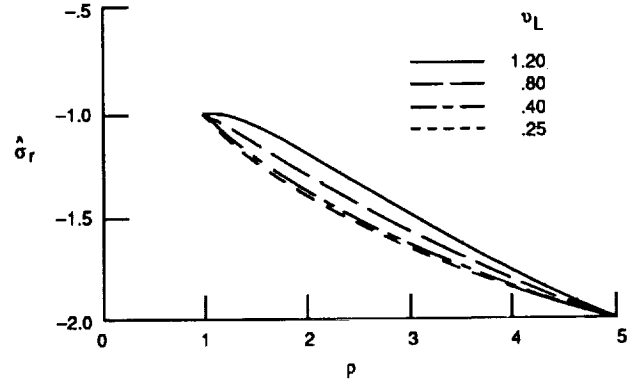


Figure 18. - Normalized radial stress versus normalized radius for varying  $\nu_L$ , i.e., 1.2, 0.8, 0.4 and 0.25, at fiber orientation of  $60^\circ$  and exterior pressure greater than interior,  $P = 2$ .

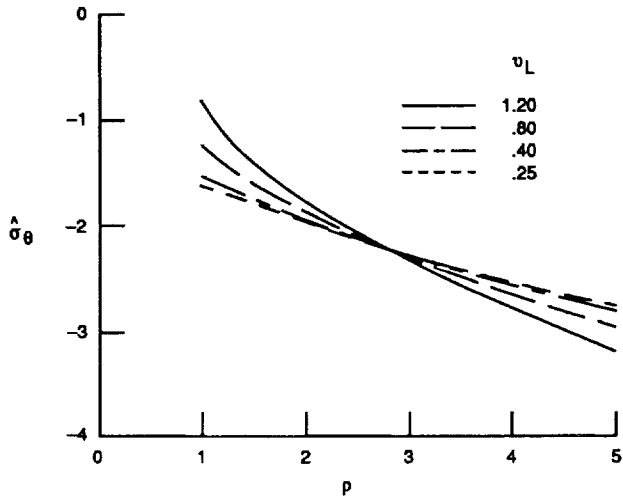


Figure 19. - Normalized tangential stress versus normalized radius for varying  $\nu_L$ , i.e., 1.2, 0.8, 0.4 and 0.25, at fiber orientation of  $60^\circ$  and exterior pressure greater than interior,  $P = 2$ .

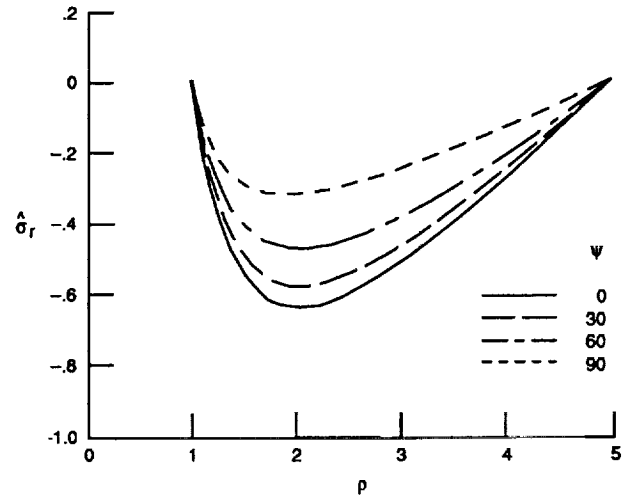


Figure 20. - Normalized radial stress versus normalized radius for fiber orientations of  $0, 30, 60$  and  $90^\circ$  when the inner surface is hotter than the outer,  $T = 0.5$ .

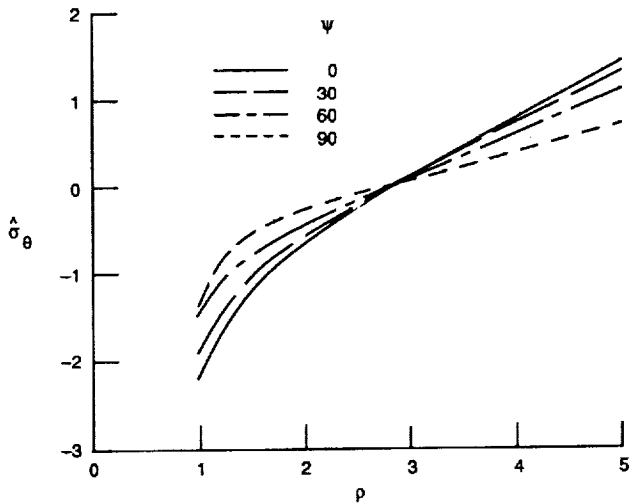


Figure 21. - Normalized tangential stress versus normalized radius for fiber orientations of 0, 30, 60 and 90° when inner surface is hotter than the outer,  $T = 0.5$ .

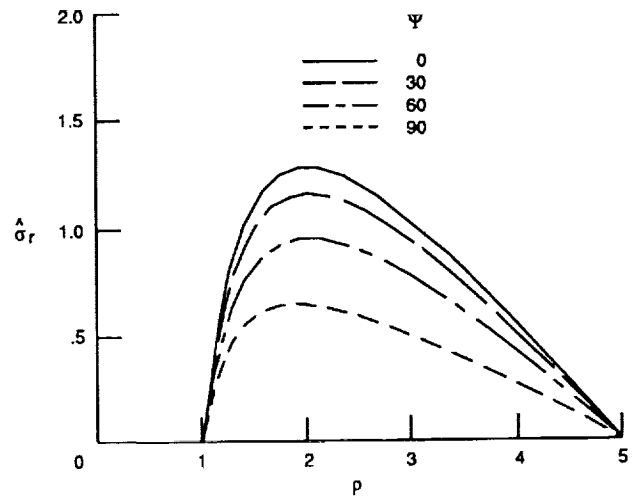


Figure 22. - Normalized radial stress versus normalized radius for fiber orientations of 0, 30, 60 and 90° when the outer surface is hotter than the inner,  $T = 2.0$ .

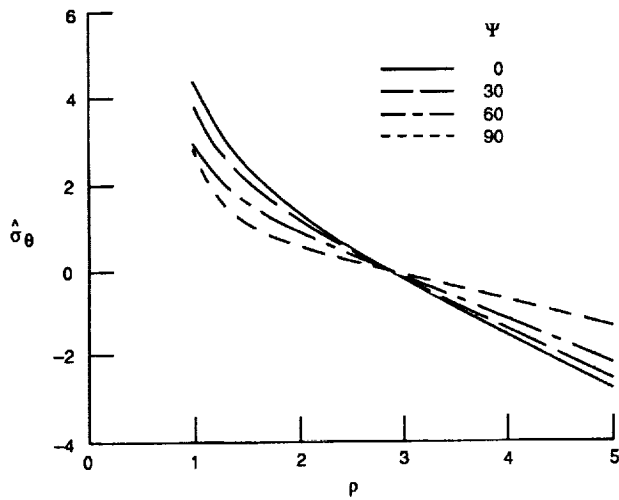


Figure 23. - Normalized tangential stress versus normalized radius for fiber orientations of 0, 30, 60 and 90° when the outer surface is hotter than the inner,  $T = 2.0$ .

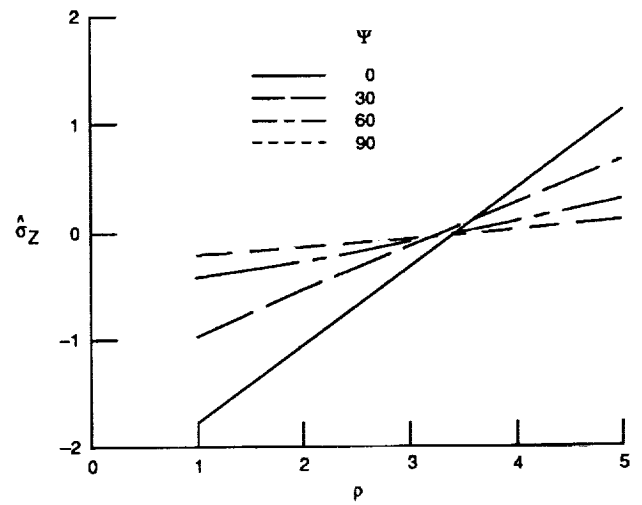


Figure 24. - Normalized longitudinal stress versus normalized radius for fiber orientations of 0, 30, 60 and 90° when the inner surface is hotter than the outer,  $T = 0.5$ .

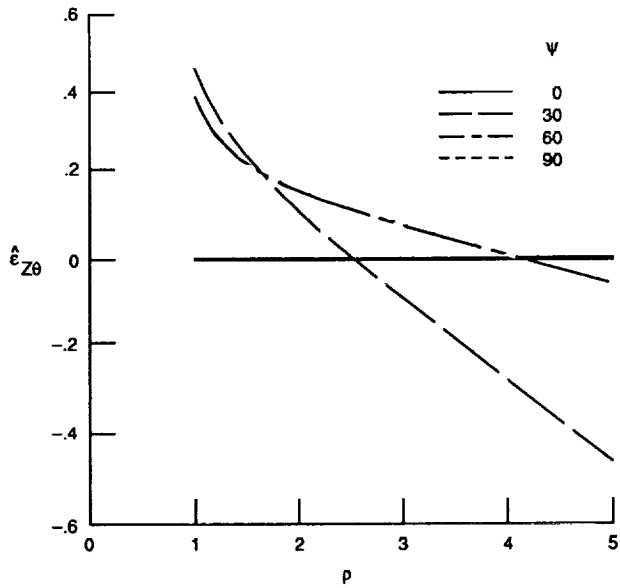


Figure 25. - Normalized shear strain versus normalized radius for fiber orientations of 0, 30, 60 and 90° when inner surface is hotter than the outer,  $T = 0.5$ .

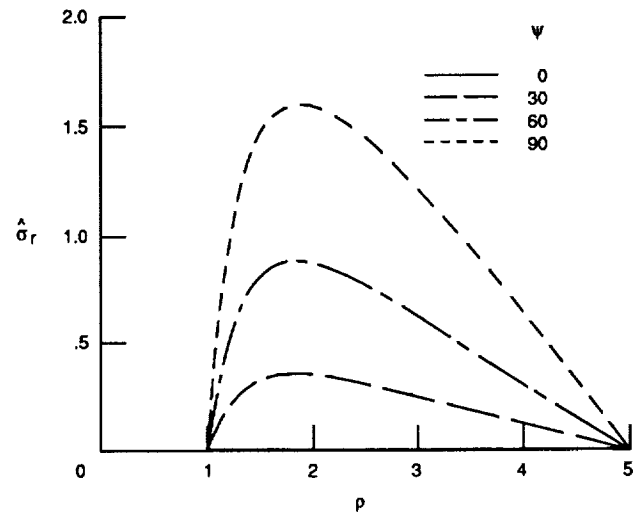


Figure 26. - Normalized radial stress versus normalized radius for fiber orientations of 0, 30, 60 and 90° for a uniform temperature distribution,  $T = 1.0, \dot{T} = 0.5$ .

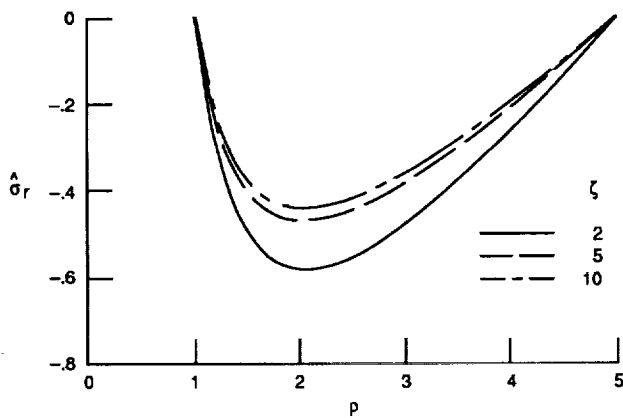


Figure 27. - Normalized radial stress versus normalized radius for varying  $\zeta$ , i.e. 2, 5, and 10 at fiber orientation of 60° when the inner surface is hotter than the outer,  $T = 0.5$ .

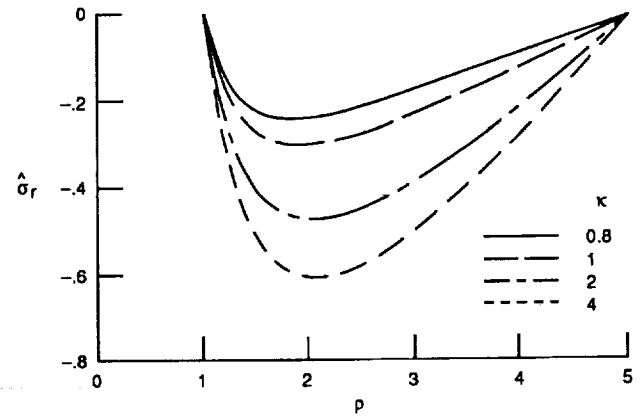


Figure 28. - Normalized radial stress versus normalized radius for varying  $\kappa$ , i.e., 0.8, 1.0, 2.0 and 4.0, at fiber orientation of 60° when the inner surface is hotter than the outer,  $T = 0.5$ .

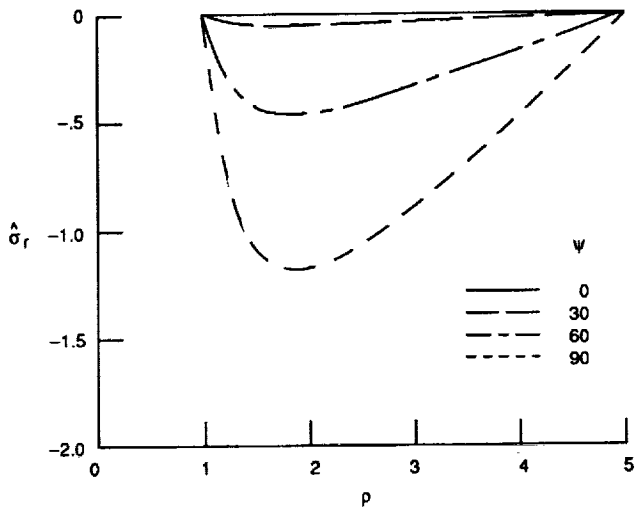


Figure 29. - Normalized radial stress versus normalized radius for fiber orientations of 0, 30, 60 and 90° for a uniform temperature distribution,  $T = 1.0$ , with  $T = 0.5$  and  $\hat{\alpha} = 0.5$

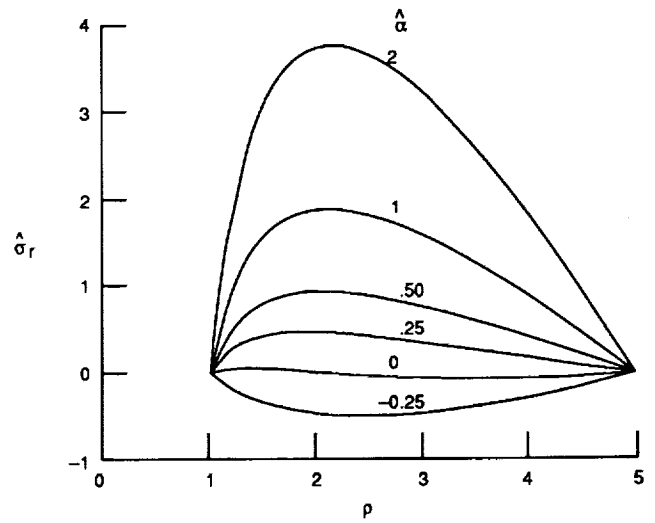


Figure 30. - Normalized radial stress versus normalized radius for varying  $\hat{\alpha}$ , i.e., -0.25, 0, 0.25, 0.50, 1.0 and 2.0, at a fiber orientation of 60° when the outer surface is hotter than the inner,  $T = 2.0$ .

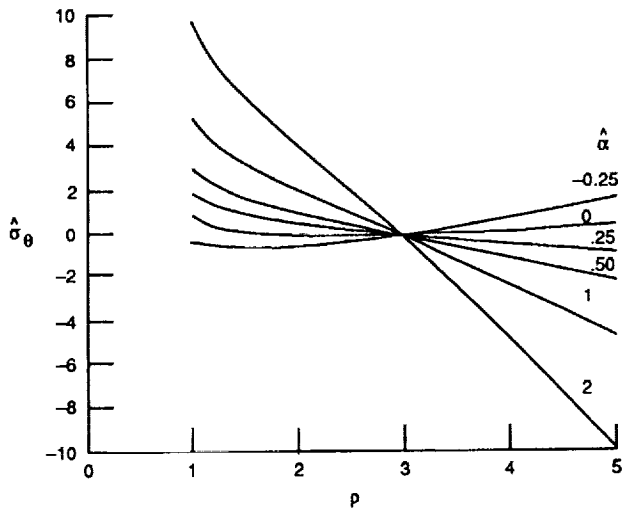


Figure 31. - Normalized tangential stress versus normalized radius for varying  $\hat{\alpha}$ , i.e., -0.25, 0, 0.25, 0.50, 1.0 and 2.0 at a fiber orientation of 60° when the outer surface is hotter than the inner,  $T = 2.0$ .

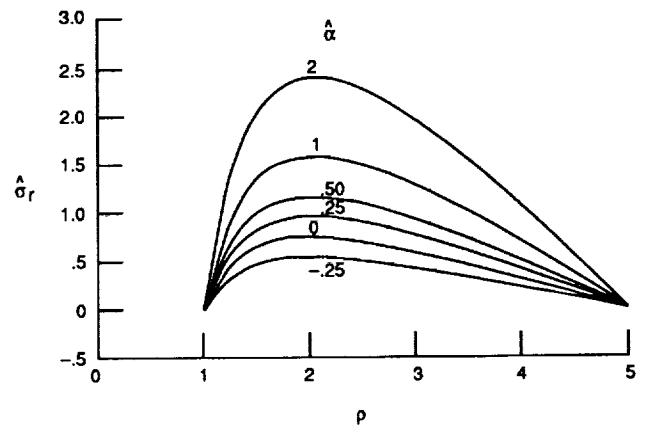


Figure 32. - Normalized radial stress versus normalized radius for varying  $\hat{\alpha}$ , i.e., -0.25, 0, 0.25, 0.50, 1.0 and 2.0, at a fiber orientation of 30° when the outer surface is hotter than the inner,  $T = 2.0$

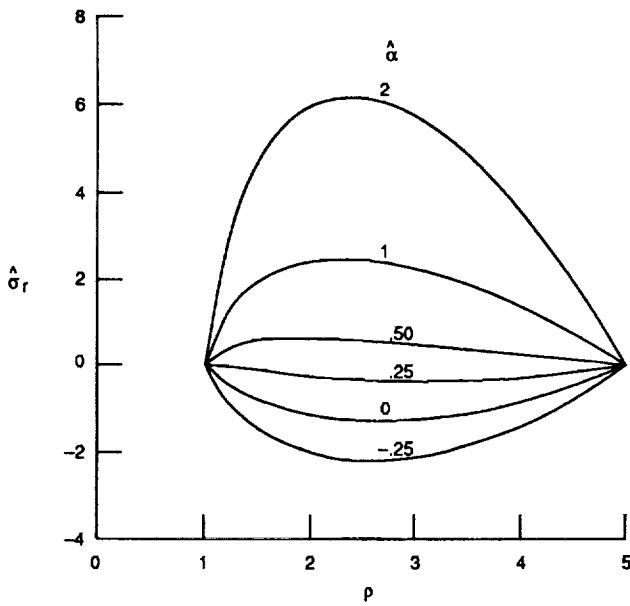


Figure 33. - Normalized radial stress versus normalized radius for varying  $\alpha$ , i.e., -0.25, 0, 0.25, 0.50, 1.0, and 2.0 at a fiber orientation of  $90^\circ$  when the outer surface is hotter than the inner,  $T = 2.0$ .

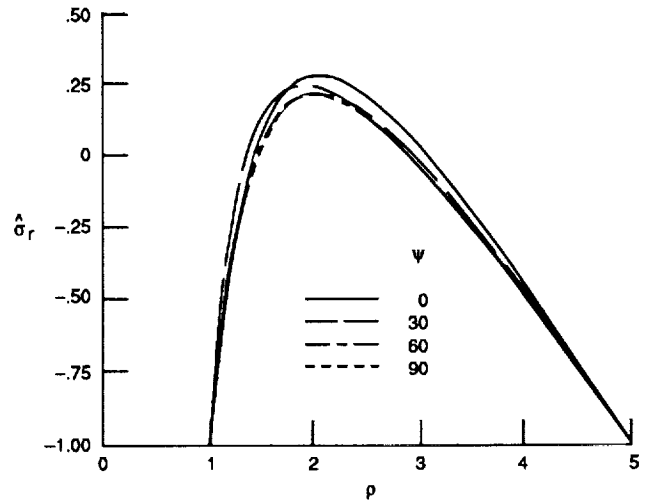


Figure 34. - Normalized radial stress versus normalized radius for fiber orientations of  $0, 30, 60,$  and  $90^\circ$  when the outer surface is hotter than the inner,  $T = 2.0$  and a uniform pressure,  $P = 1.0$ .

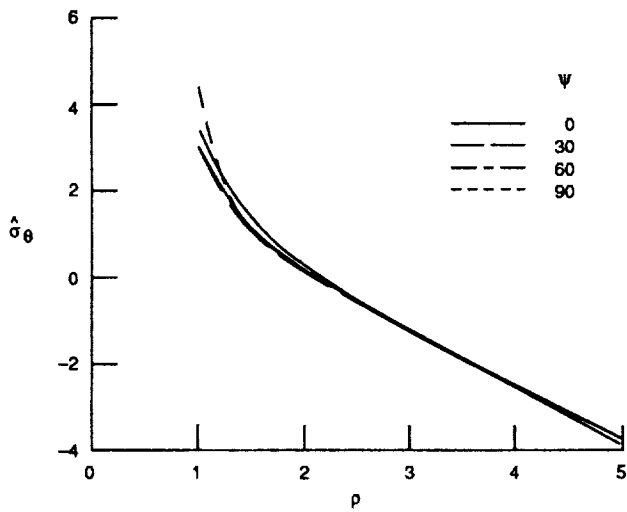


Figure 35. - Normalized tangential stress versus normalized radius for fiber orientations of  $0, 30, 60,$  and  $90^\circ$  when the outer surface is hotter than the inner,  $T = 2.0$  and a uniform pressure,  $P = 1.0$ .

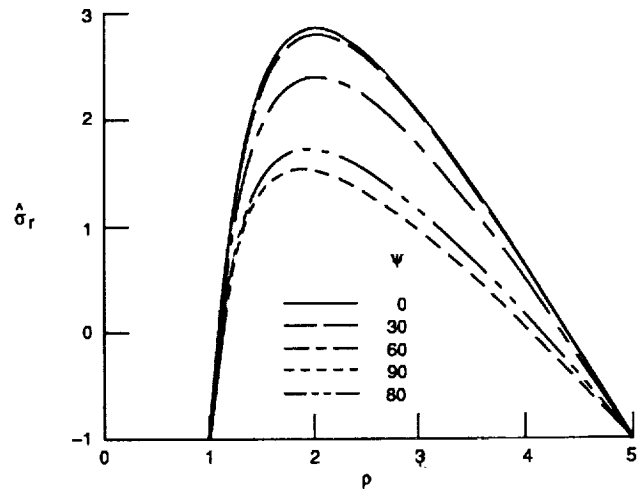


Figure 36. - Normalized radial stress versus normalized radius for fiber orientations of  $0, 30, 60,$  and  $90^\circ$  when the outer surface is hotter than the inner,  $T = 4.0$  and a uniform pressure,  $P = 1.0$ .

1. Report No. NASA TM-102320		2. Government Accession No.		3. Recipient's Catalog No.	
4. Title and Subtitle A Thermoelastic Transversely Isotropic Thick Walled Cylinder/Disk Application: An Analytical Solution and Study				5. Report Date October 1989	
				6. Performing Organization Code	
7. Author(s) S.M. Arnold				8. Performing Organization Report No. E-5016	
				10. Work Unit No. 510-01-0A	
9. Performing Organization Name and Address National Aeronautics and Space Administration Lewis Research Center Cleveland, Ohio 44135-3191				11. Contract or Grant No.	
				13. Type of Report and Period Covered Technical Memorandum	
12. Sponsoring Agency Name and Address National Aeronautics and Space Administration Washington, D.C. 20546-0001				14. Sponsoring Agency Code	
15. Supplementary Notes					
16. Abstract  A continuum theory is utilized to represent the thermoelastic behavior of a thick walled composite cylinder that can be idealized as transversely isotropic. A multiaxial statement of the constitutive theory employed is presented, as well as, the out of the plane of isotropy, plane stress and plane strain reductions. The derived analytical solution presented is valid for a cylindrical tube or thin disk with a concentric hole, subjected to internal and/or external pressure and a general radial temperature distribution. A specific problem examined is that of a thick walled cylinder subjected to an internal and external pressure loading and a linear radial temperature distribution. The results are expressed in nondimensional form and the effects on the response behavior are examined for various material properties, fiber orientation and types of loadings.					
17. Key Words (Suggested by Author(s)) Thermoelastic; Composites; Transverse isotropy; Thick walled cylinder; Analytical solution			18. Distribution Statement Unclassified - Unlimited Subject Category 39		
19. Security Classif. (of this report) Unclassified		20. Security Classif. (of this page) Unclassified		21. No of pages 44	22. Price* A03